A 3-D Numerical Model for Pullout Capacity of Single Batter Piles in Sand

Mehmet Atici

A Thesis

in

The Department

of

Building, Civil and Environmental Engineering

Presented in Partial Fulfillment of the Requirements

For the Degree of Master of Applied Science (Civil Engineering) at

Concordia University

Montreal, Quebec, Canada

March 2009

Your file Votre référence
ISBN: 978-0-494-63247-5
Our file Notre référence
ISBN: 978-0-494-63247-5

ABSTRACT

A 3-D Numerical Model for Uplift Capacity of Single Batter Piles in Sand

By Mehmet Atici

Pile foundations are usually recommended when soil capacity is not sufficient for the expected loads of the structure with conventional foundation techniques. While the case of vertical piles is reasonably documented in the literature, the case of batter piles in sand has received little attention from the researchers. This is mainly due to the complexity of modeling the earth pressure distribution around the pile's shaft. Attempts were made to model the pullout behavior of vertical piles numerically using two-dimensional approaches, which does not represent the field condition and accordingly the results are scattering.

In this study a 3D numerical model was developed to investigate the uplift capacity of single batter piles in sand. The model utilizes the powerful software "ABAQUS" version 6.6, which is capable to model such complex interaction in three-dimensional stress analysis. The model was validated with the prototype test results of Hanna and Afram (1986) and field work of Alewnah (1999)

Design procedure and design charts have been presented to assist foundation engineers to predict the uplift capacity of batter piles in sand.

ACKNOWLEDGEMENT

I would like to express my gratitude to my supervisor Dr. Adel Hanna for his patient guidance, encouragement, and financial support throughout this study.

I am thankful to Dr. Taher Ayadat for his critical advices during the course of the thesis.

I also thank my colleagues Mr. Sherif Soliman and Mr. Alp Enginsal for their support to conclude this study.

Finally, I take this opportunity to express my profound gratitude to my beloved parent and my wife for their moral support and patience during my study at Concordia University.

TABLE OF CONTENT

LIST OF FIGURES

LIST OF TABLES

LIST OF SYMBOLS

Net ultimate uplift	$Q_{(un)}$
Lateral earth pressure coefficient	K
Perimeter x length of pile embedment	A_s
Average vertical effective stress	$\overline{\sigma_v}$
Angle of friction	ϕ
Unit weight of soil	γ
Depth	z
Pile Diameter	D
Pile Perimeter	P (or c)
Pile Length	L
Soil-pile friction angle	δ
Total passive earth pressure acting on the pile shaft	P_p
Own weight of the pile	W_e
Net uplift capacity factor	A_1
Coefficient of earth pressure	K_s
Average coefficient of earth pressure	K_{ave}
Initial coefficient of earth pressure	Ki

Coefficient of earth pressure at Rest	Ko
Exponential decay rate	μ
Power decay rate	n
Shear stress	τ
Soil Cohesion, perimeter (Chapter III)	c
Inclination	α
Shaft Resistance	Qs
Reduction Factor	R
Reduction Factor	R_2

CHAPTER I

INTRODUCTION

1.1 GENERAL

Piles are often used to support heavy loads or to reduce settlement of the foundation. Advancement of pile materials and driving techniques started over 5000 years ago and continued to progress from wooden section to precast and pre-stressed concrete until modern times.

With the rise of the Roman Empire, researchers developed timber pile techniques in Europe, Asia, and Africa and implemented them for bridges, piers, or passage ways built by Roman builders to help the army to mobilize faster. Until the end of 18^{th} century these techniques were still primitive; nevertheless, opened a new era in foundation engineering.

Since then, continuous developments were reported in the design and the method of installation of these piles. New technologies allowing builders to drive numerous piles started during $18\text{-}19^{th}$ century in England and Germany as well as Russia, Kronstadt Forts. During the 18^{th} Century, the French Military-Engineer Perronet proposed the augers system for exploring subsoil conditions; since then, research in this matter was commenced.

1.2 BATTER PILES

Batter piles are often recommended to support high-rise buildings, offshore structures, and towers where the foundation could be subjected to uplift or compressive loading.

Figure 1.1 (a, b) illustrates a typical offshore structure and electrical tower supported on batter pile foundation.

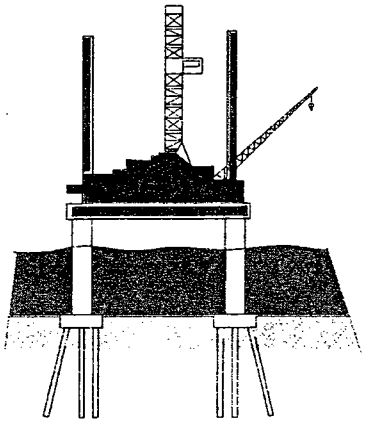

Figure 1.1. a Offshore Structure

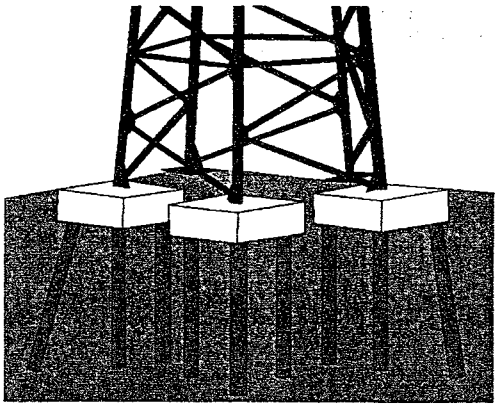

Figure 1.1. b Electrical tower foundation

Batter piles are installed in the direction of the expected load, to resist high overturning moments due to horizontal loads such as wind, wave and ship impact.

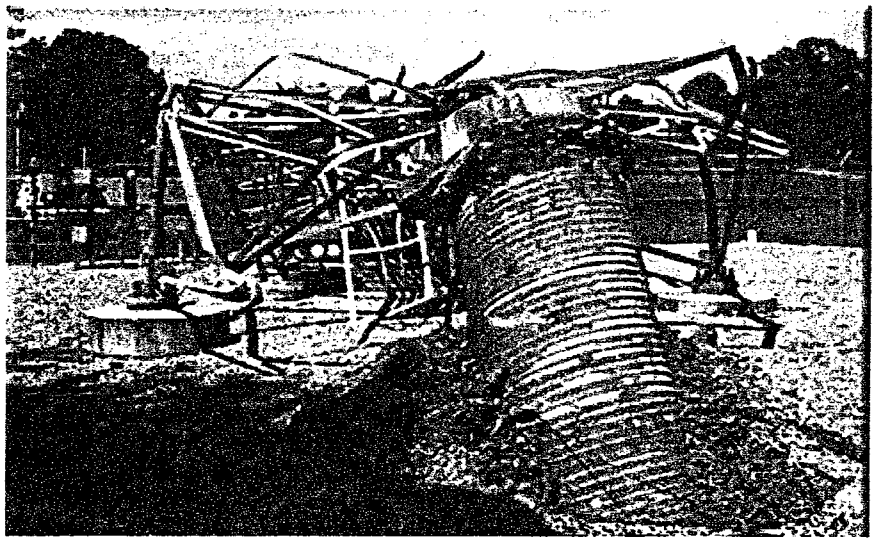

Figure 1. 2 Foundation failures due to pullout forces (Reference 17)

Figure 1.2 demonstrates the importance of pullout forces on pile systems, subject, which researchers have neglected for many years. Only in 20^{th} century, studies began seriously investigating shaft resistance for vertical and thereafter batter piles.

1.3 OBJECTIVE AND SCOPE OF THE WORK

The objective of this study is to develop a 3-D numerical model to examine shaft resistance of a single batter pile in sand during pullout. After validation of the numerical model, results will be produced for a wide range of parameters, which believed to govern this behavior.

In Chapter 2, literature review will be presented from numerous previous studies related to this subject. Each study will be summarized and followed by a discussion. In Chapter 3, a 3D numerical model will be developed to simulate problem stated. In Chapter 4 design charts for estimating the shaft resistance for these piles will be presented. Chapter 5, conclusion and recommendations will be given for future studies.

CHAPTER II

LITERATURE REVIEW

2.1 BACKGROUND

Ireland (1957), has conducted 6 field pull-out tests along the coast of Florida. According to the results he obtained, he suggested the following formula to determine the uplift capacity of vertical piles.

$$Q_{(un)} = KA_s\overline{\sigma}_v \tan\phi \qquad (2.1)$$

Where:

$Q_{(un)}$= Net ultimate uplift

K=Lateral earth pressure coefficient

A_s=Perimeter x length of pile embedment

$\overline{\sigma}_v$ =Average vertical effective stress

ϕ = Angle of shearing resistance

The net ultimate uplift capacity was taken as the difference between gross uplift capacity and pile's self weight. When the soil is dry and homogenous, the average effective stress at any depth can be determined as follows:

$$\overline{\sigma}_v = \frac{\gamma z}{2} \qquad (2.2)$$

Where:

γ= Unit weight of soil

z= Depth

Ireland recommended an average value of 1.75 for the lateral earth pressure coefficient (K). If the perimeter and embedded length of the pile are defined p and L respectively, the equation can be written as:

$$Q_{(un)} = 0.875 p \gamma L^2 \tan\phi \qquad (2.3)$$

Vesic (1970) reported that local shaft friction at any level changes with pile penetration depth, which was an important outcome that has been neglected to this point. As seen in Figure 2. 1 skin friction varies along the pile length.

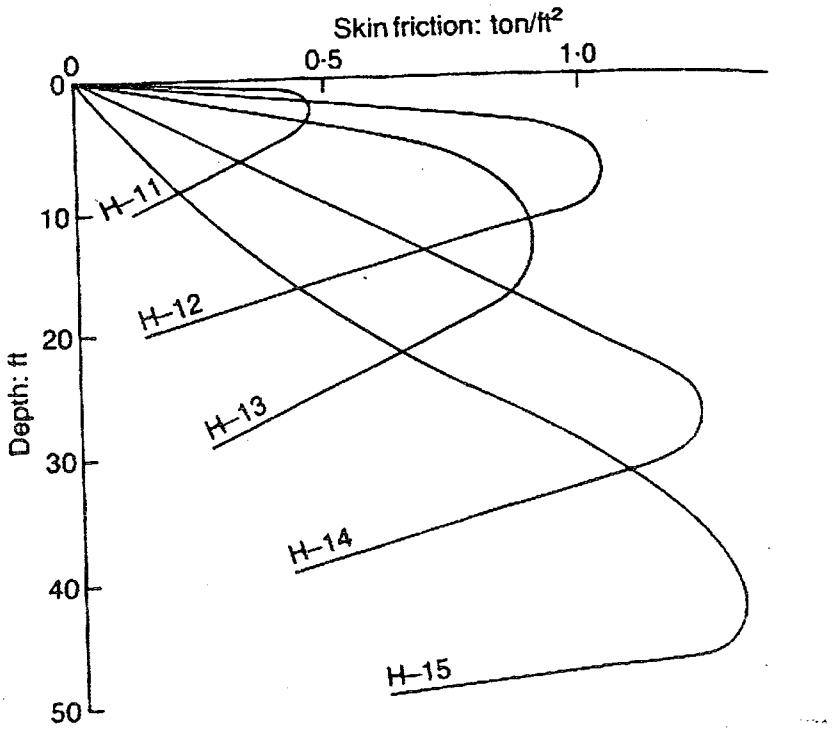

Figure 2. 1 Skin Friction versus depth of pile, after Vesic (1970)

These finding have encouraged researchers to further investigate the pile drivability and its friction fatigue. Note that symbol H refers to type of the pile section.

Meyerhof (1974) published a study for uplift capacity of vertical piles subjected to axial loads. Shortly after, he extended his study for vertical piles subjected to inclined loads.

In the case of vertical piles, Meyerhof suggested the following formula for the uplift capacity of these piles.

$$Q_{(un)} = \frac{1}{2}\gamma K_b L^2 D \qquad (2.4)$$

where: K_b is the uplift coefficient, which is given in Figure 2. 2. K_b is a function of the embedment ratio (L/D) and the soil friction angle.

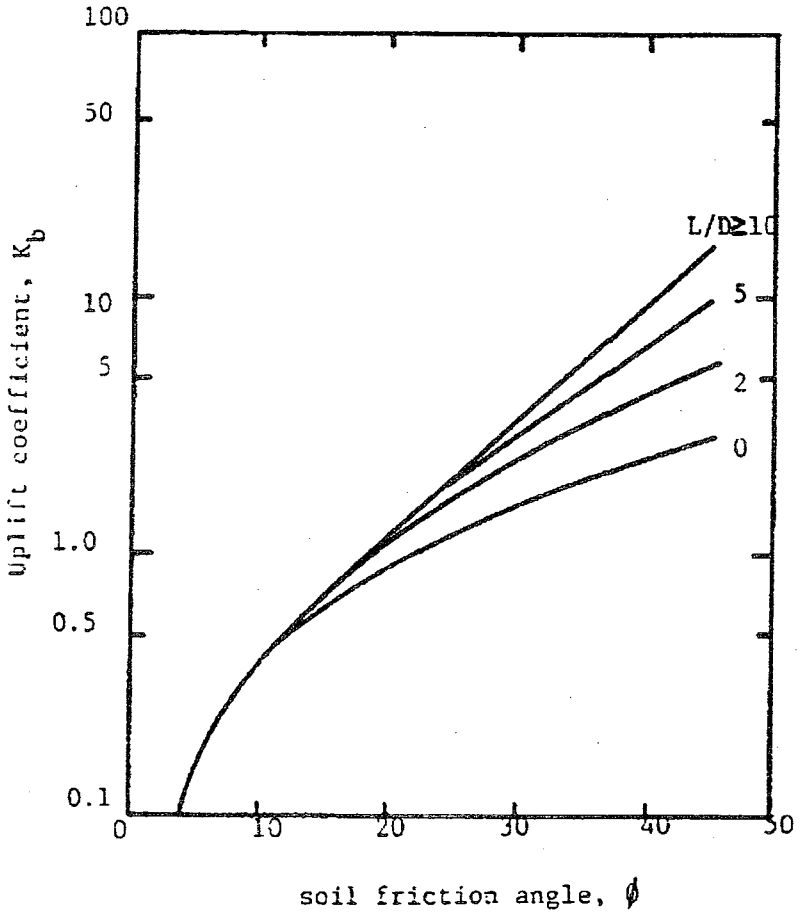

Figure 2. 2 Soil Friction angle vs Uplift Coefficient, after Meyerhof (1974)

For batter driven piles having an inclination angle between 0° and 90° with the vertical, Meyerhof suggested the following formula to predict the pullout capacity.

$$Q_{(ug)\alpha} = Q_{(un)\alpha} + W\cos\alpha \tag{2.5}$$

Meyerhof also presented the following formula for bored piles.

$$Q_u = K_u p L^2 \overline{\sigma_v} \tan\delta \tag{2.6}$$

Where:

K_u=Uplift coefficient

δ=Soil-pile friction angle

For Circular Piles,

$$p = \pi.D \tag{2.7}$$

$$\overline{\sigma_v} = \frac{\gamma.L}{2} \tag{2.8}$$

Furthermore:

$$Q_u = K_u.\frac{\pi}{2}.D.\gamma.L^2.\tan\delta \tag{2.9}$$

The uplift coefficient, K_u values can be determined from Figure 2. 3, as a function of the angle of friction (ϕ).

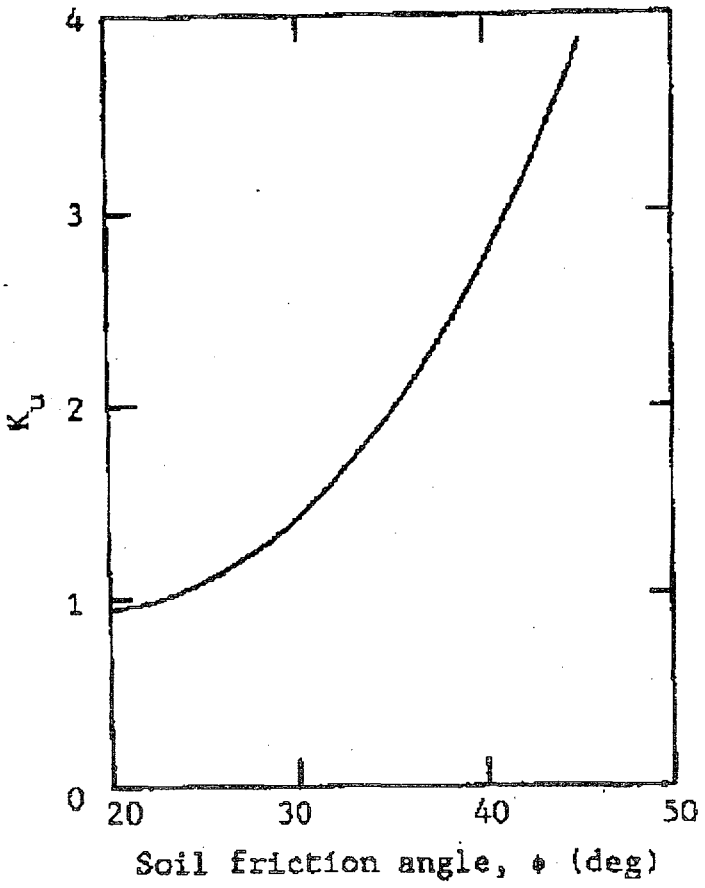

Figure 2. 3 Friction Angle vs. Uplift Coefficient; after Meyerhof (1974)

Meyerhof then extended his theory for the case of inclined loads as shown in Figure 2.4.

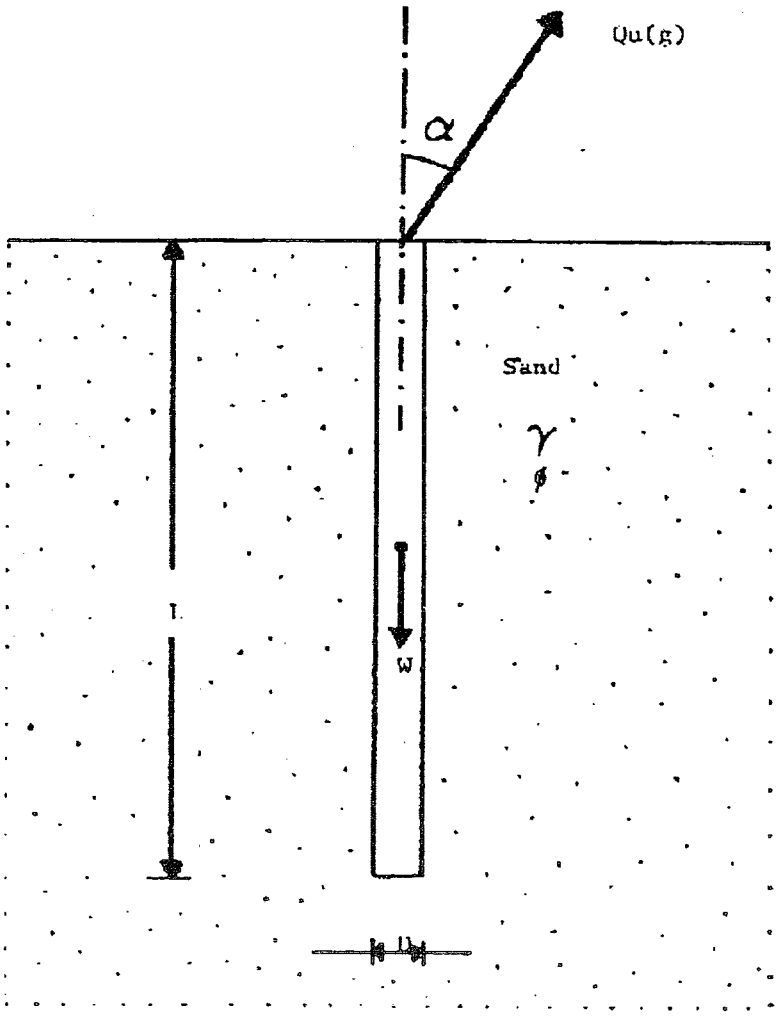

Figure 2. 4 Pullout capacity at inclined loading, Meyerhof (1974)

Hanna and Aram (1986) conducted an experimental study to investigate the case of pullout capacity of single vertical and batter piles in sand. They tested steel piles 38mm and 76mm in diameter at different inclinations. They presented the following formula:

$$P_u = P_p \sin \delta \pi D + W_p \qquad (2.10)$$

Where:

P_p= Total passive earth pressure acting on the pile shaft.

D= Pile Diameter

W_e= Own weight of the pile

δ= the mobilized angle of wall friction at soil-pile interface

Hanna and Afram reported that pull-out capacity of batter piles decreases due to the increase of pile inclination. They then presented the following formula for battered pile having an inclination angle of α;

$$P_{u\alpha} = P_u \cos\frac{\alpha}{2} \tag{2.11}$$

Where:

α= angle of inclination of pile with vertical $\left(0^0 \le \alpha \le 30^0\right)$

$$P_{u\alpha} = \frac{\gamma}{2}\pi D L^2 K_{u\alpha} + W_p \cos\alpha \tag{2.12}$$

Where:

γ= Unit weight of sand

$K_{u\alpha}$= Uplift coefficient for batter piles

L= Length of pile

Chattopadhyay and Pise (1986), presented the results of an analytical study to determine the uplift capacity of piles embedded in sand. The study considered the length, diameter, and surface characteristics of piles as well as soil properties.

The authors generated a model of vertical pile of diameter, D, and embedded portion of pile length, L, surrounded by soil having an frictional angle of, ϕ, and effective unit weight, γ; Figure 2. 5.

Using "limit equilibrium analyses", the ultimate capacity of the pile was predicted based on following assumptions.

1. The shape and extent of the surface depend on the slenderness ratio, λ the angle of shearing resistance ϕ of the soil, and the pile friction angle δ.
2. For pile friction angle δ=0, under ultimate uplift force, P_u, the resulting failure surface initiates tangentially to the pile surface at the tip of the pile and moves through the surrounding soil.
3. For δ>0, the inclination of the failure with the horizontal at the ground surface approaches (45-$\phi/2$) while for δ=0, is at 90^0

The authors presented a non-dimensional formula to predict the uplift capacity of pile:

$$\frac{P_{u(n)}}{\frac{\pi D^2}{4}\gamma L} = 2K_s \tan\delta.\frac{L}{D} = 4A_1(\frac{L}{D}) \qquad (2.13)$$

$$K_s = 2A_1 / \tan\delta \qquad (2.14)$$

$$A_1 = (1-\sin\phi)\tan\delta/2 \qquad (2.15)$$

Where:

A_1=net uplift capacity factor

K_s=coefficient of earth pressure

The formula is not widely used in practice as the pile's diameter is not taken into consideration in evaluating the coefficient of earth pressure "K_s".

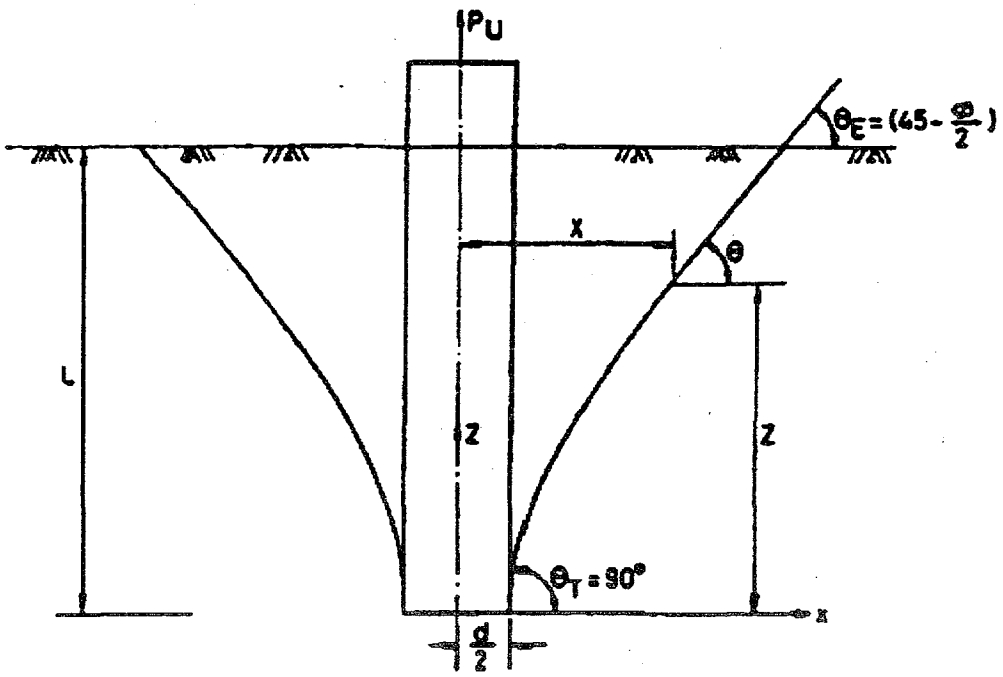

Figure 2. 5 Failure mechanism; after Chattopadhyay and Pise (1986)

Kraft (1990), has presented another design method to estimate the earth pressure coefficient based on the relative density of the soil and the effective area ratio of the pile.

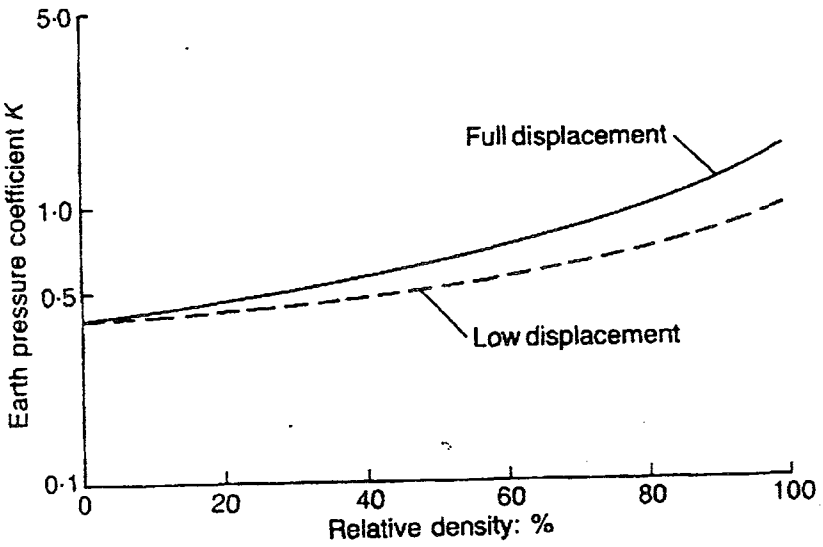

Figure 2. 6 Earth Pressure Coefficient versus Relative Density; after Kraft (1990)

In developing the theory, the author used field data, assuming the pile-sand interface angle, $\delta=0.7\,\phi_{max}$ for silica sands and calcareous sands, $\delta=0.7\,\phi_{max}$ where ϕ_{max} is defined as the peak effective friction angle for the soil.

The relative density of soil presented in Figure 2. 6 is independent of the soil grain size. This assumption had lead to disagreement with the laboratory results of Kishida & Vesugi (1987) and Jardine et al (1992).

Leathers (1994), studied deformations and lateral movement of the sand layer during pile driving. The piles driven in the construction site were 36cm, square, and precast concrete sections with ranging from 29 to 39m in length.

The average value of volumetric densification of sand stratum was ranging 1.4% to about 1.7%. Larger densification occurred in medium sand.

Ergun and Akbulut (1995), proposed an interesting solution to increase shaft resistance, as demonstrated in Figure 2.7. A model shaft-expanded pile driven into sand was tested under axial compression load. To increase the shaft resistance, they used flaps on different elevations attached to the body of pile.

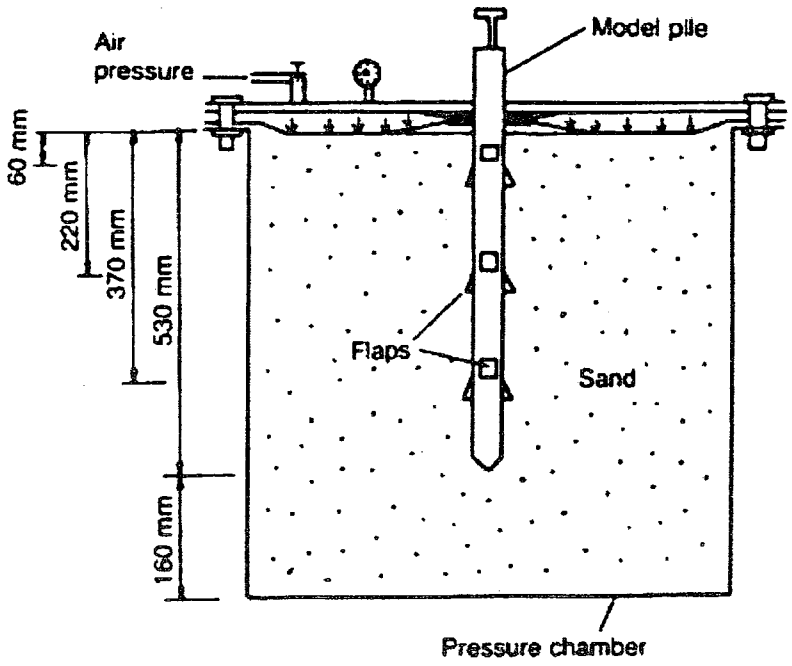

Figure 2.7 Pile Setup of Ergun and Akbulut (1995)

They reported that shaft expansion can increase the pile capacity by more than 100 % in some cases, which is quite significant.

Jardine et al (1996) investigated time-related increases in shaft resistance of driven piles in sand. Based on the results of the field pullout test, they concluded that shaft resistance can surprisingly increase up to 85% over five years. They attributed this change to long-term sand creep referring arching mechanism around pile.

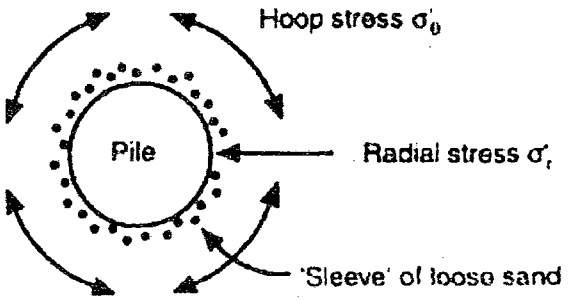

Figure 2. 8 Arching mechanism around the pile's shaft, after Jardine et al (1996)

Long-term sand creep would reduce the arching effect allowing σ'_{rc}, radial effective stress after installation. Intense sand compaction at the tip during driving can create a thin sleeve of looser sand. High hoop stress σ'_o could then be sustained in the surrounding denser sand by arching as shown in Figure 2. 8.

Alawneh (1999), proposed a method to estimate the ultimate uplift capacity of piles in sand based on a database of pullout pile tests in literature. He focused on determining the earth pressure coefficient $K_{(z)}$ at ultimate pullout load. He presented the following formula, which presented in graphical form in Figure 2. 9.

$$K_{(z)} = K_{(\min)} + (K_{(\max)} - K_{(\min)})\left[\frac{1}{4}\left(\frac{L-z}{D}\right)\right]^{-n} \qquad (2.16)$$

$$\left(\frac{L-z}{D}\right) \geq 4 \qquad (2.17)$$

Where;

D: Pile diameter

μ: exponential decay rate

n: power decay rate

Although his results were in ± 30% error band, this method was considered an accepted solution for design purposes.

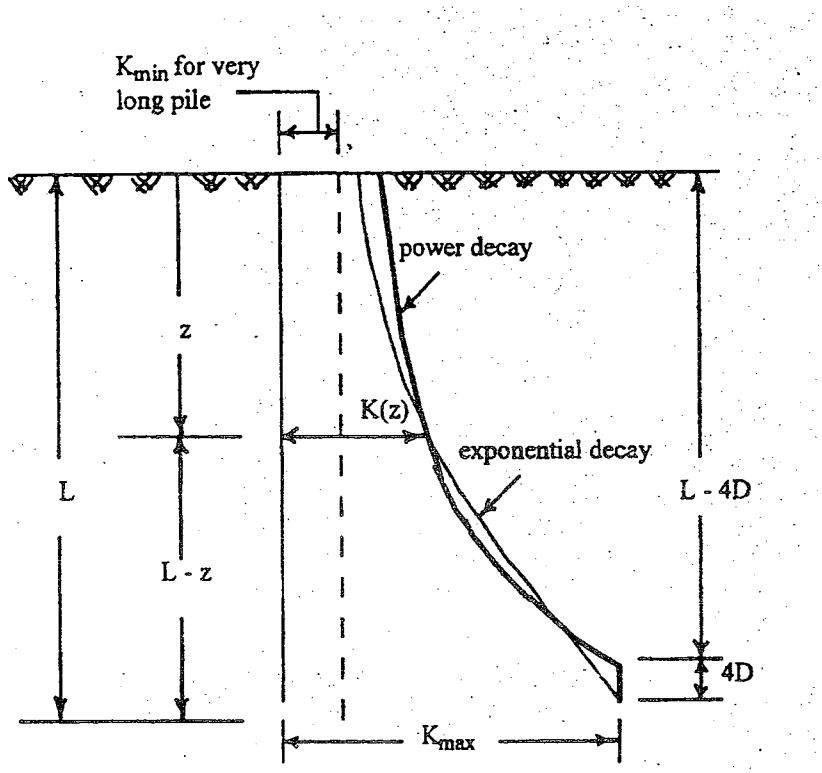

Figure 2. 9 Earth Pressure Distribution; after Alewnah 1999

Malkawi, Shlash and Al-Deeky (1999), describe the different factors affecting the ultimate uplift capacity of piles in sand. They reported that the net shaft resistance depends on:

- The type of pile end: Open or Closed Ended Piles
- Pile texture
- Pile size
- Placement Method: Driving, jacking
- Soil density

Authors investigated and evaluated each factor separately, and ranked them as the most effective one to the less effective factors governing the shaft resistance as sand density, pile replacement method, pile texture, and pile type.

The study has shown that driving method yield higher shaft resistance than jacking. In addition, closed-ended model piles exhibited 24% higher in shaft resistance at ultimate uplift. Although pile's diameter solemnly influences the ultimate pile capacity, they did not take it into account in this study.

Gavin and Lehane (2003), investigate factors affecting the capacity of open-ended (pipe) piles in sand. They reported that the majority of existing methods in the literature are empirical or using parameters, which established from test results as demonstrated in Figure 2. 10.

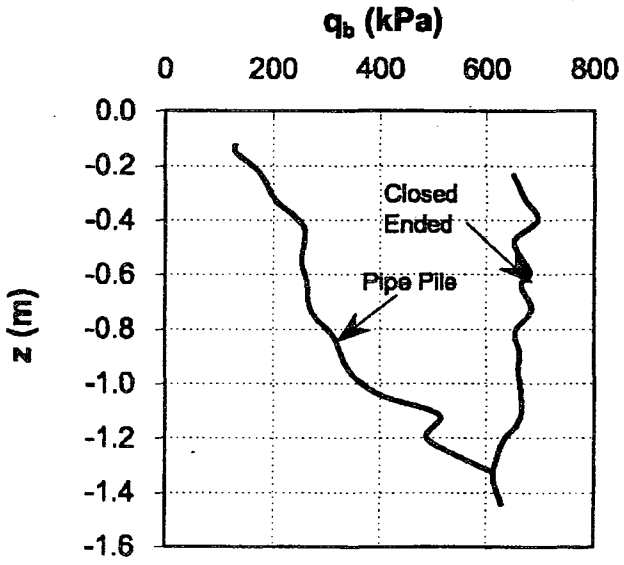

Figure 2. 10 Average end bearing stress for piles in compression in sand;

Although authors stated that open or closed end shows significant difference as far as end bearing is concerned, shear stresses that can be develop between the sand plug and internal pile wall during tension are quite small to be relied on.

Hanna and Nguyen (2003) conducted experimental investigation on single batter piles in sand. They measured the earth pressure distribution on the pile's shaft (Figure 2. 11) and developed a theory to predict the pullout capacity of these piles. They also reported that due to an increase of the pile inclination angle, α, the unit shaft resistance decreases.

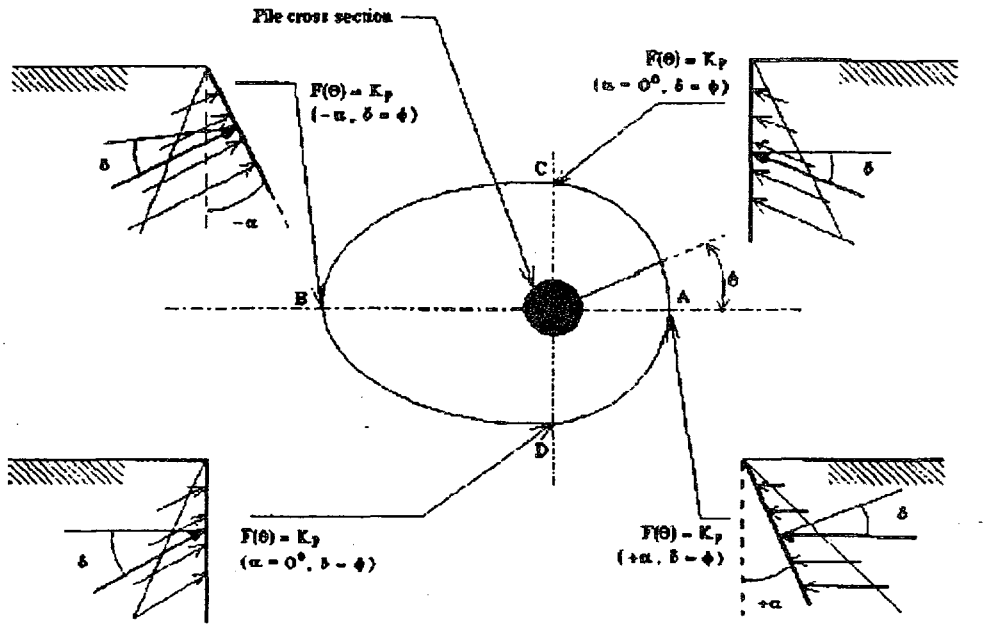

Figure 2. 11 Earth Pressure Distribution on the pile's shaft; after Hanna and Nguyen (2003)

Alawneh, Nusier, and Al-Kateeb (2003), collected the field data for 30 pullout pile load tests to examine the dependency of unit shaft resistance on effective vertical stress. The authors reported on the effect of pile length on the pullout capacity (Figure 2. 12), however they did not report on role of the pile inclination.

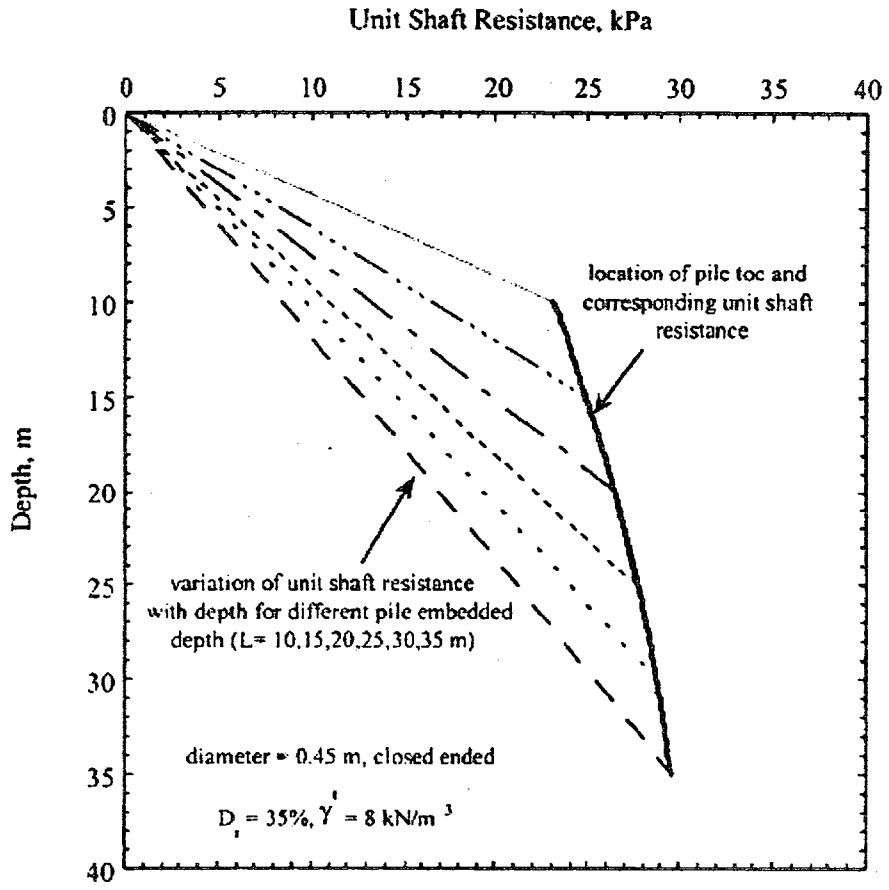

Figure 2. 12 Variation of local unit shaft resistance with depth for different pile penetration

2.1 DISCUSSION

Several reports can be found in the literature with respect to shaft resistance for vertical piles in sand. Amount of work reported for the case of battered piles is insufficient. Nevertheless, with the exception of Hanna and Nguyen (2003) no attempts were made to evaluate the earth pressure distribution on the pile's shaft for battered piles, which depend on:

- Strength and deformation characteristics of the sand
- Initial stress conditions
- Pile installation technique
- Pile material, shape and size

As presented above, Alewnah (1999) suggested an assumed distribution of earth pressure coefficient along the pile's shaft by accepting an error range of 30%, which is not a proper practice. The results reported by Gavine and Lahane (2002) are limited to open-end or closed-end piles, yet, they did not examine the effect of the pile installation techniques on the pile capacity.

For batter piles some researchers claim effect of angle is significant while others thought it is negligible. Accordingly, research on the subject is warranted.

CHAPTER III

NUMERICAL MODEL

3.1 GENERAL

In this chapter, the case of single battered piles driven in cohesionless soil will be analyzed using finite element technique. There are many commercial types of software available in the market. However the selected software must have following features:

- 3-Dimensional modeling
- Ability to model interface elements and interactions
- Auto-Mesh Control
- Ability to select different types of elements

Finite element method of analysis is widely used to simulate soil stress-strain characteristics of a variety of geotechnical engineering problems. "ABAQUS" is a highly sophisticated 2D-3D program capable of providing features mentioned above as well as characterizing static, dynamic, thermal, and acoustic cases with linear or nonlinear solutions.

3.2 NUMERICAL MODEL

In this section, a three dimensional finite element model is developed for the case under investigation. In developing this model, distinctive characteristics which influence the outcome of the analysis have been considered individually in order to achieve the best and most accurate results. These are element types, degrees of freedom, number of nodes and the material, constitutive law.

3.2.1 Element Type

Figure 3. 1 presents 3D "finite" solid element with different nodal options. It will be practical to define the soil element as infinite or very fine-meshed elements. However, under these circumstances it will be difficult rather impossible to obtain sensible results.

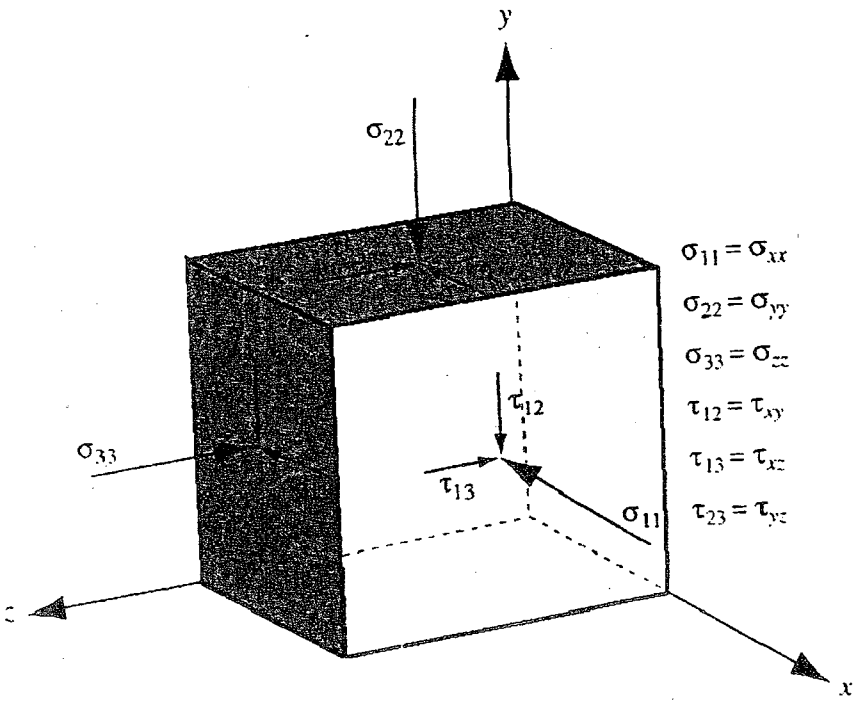

Figure 3. 1 Stress Components on a finite soil cube After Helwany (2007)

Meshing 3D elements can sometimes be challenging, depending on the type of element is used and the size in the region, where stress and deformation are expected to be relatively high. Figure 3. 2 present element families for Finite Element Modeling (FEM). While, automatic meshing might lead to errors, tetrahedron elements with solid part can sufficiently be meshed without using partitions. Thus in this investigation, a 4-

node linear tetrahedron, with hourglass control will be used in the present numerical model.

Hour-glassing defined as a numerical facility, causing linear reduced-integration elements to behave more flexible. Reduced integration, i.e., assigns 4 integration nodal points instead of 8 to calculate the necessary stress-strain components of the mesh unit single surface. While using a lower-order integration technique for the element stiffness, the mass matrix and the loads use full integration. Reduced integration diminishes running time, especially in three dimensional analyses. It can also be noted that fully integrated linear elements should be used only when expected that the loads will produce minimal bending. Accordingly, in this investigation, linear reduced-integration elements will provide acceptable results condition that the model is well meshed.

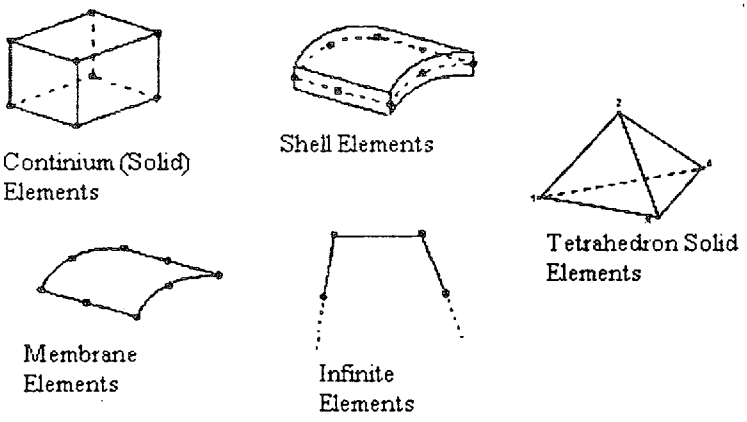

Figure 3. 2 Element Families for Finite Element Modeling-ABAQUS Manual (2006)

Quadratic elements are usually subjected to complicated states of stress, which is regarded as one of the advantages is that they display high resistance to locking. Locking prevents elements to move freely creating an incompressible element. In this

investigation quadratic elements will be used as they are considered the appropriate solution for stress-displacement systems for most of the cases unless the solid part has irregular geometry where partitions should be created in the solid. Yet, in order to save on operating time, tetrahedron element (Figure 3. 3) is considered the best solution together with its free-meshing option.

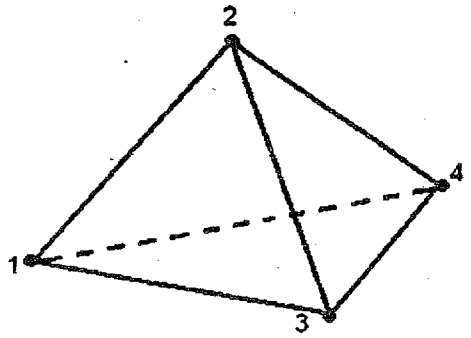

Figure 3. 3 Tetrahedron Element nodes

For tetrahedral elements the normalized shape factor is defined as the ratio of element volume to optimal element volume. Element volumes are automatically assigned by free-meshing. Optimal element volume is the volume of an equilateral tetrahedron with the same circumradius as the element. The circumradius is the radius of the sphere passing through the four vertices of the tetrahedron. Free meshing values will be mentioned in title "Soil Constitutive Model".

3.2.2 Boundary Conditions

Boundary conditions are to define soil faces hence mesh-units in the system matrix. This will allow user to create and assign degrees of freedom to the single unit[1]. Other part of

[1] A single unit is a part of soil or pile as a particle.

the model can be sufficiently meshed to transfer stresses from one node to another. In this investigation, step application will be used to establish the boundaries of the model, as described in Figure 3. 4.

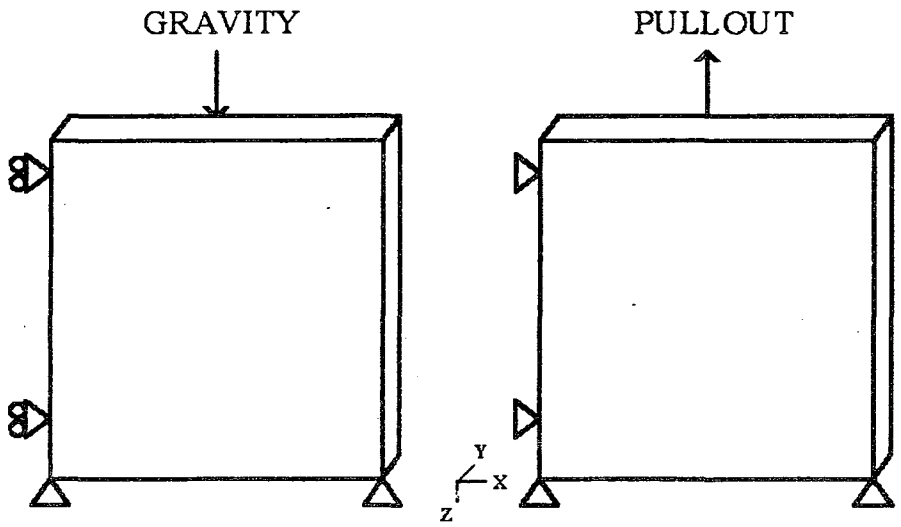

Figure 3. 4 Load Application and Boundary Conditions

Application of gravity causes stresses on the soil part. Restraining the bottom of the mesh, as shown on Figure 3. 4 will allow the soil to settle downward (on the z direction) without having a bulging effect. On the contrary, restraining two opposite sides will affect degree of freedom and hence the results.

In 1977 Randolph suggested the use of an axisymetric mesh (Figure 3. 5) having a width of minimum of 50 times the pile's diameter and depth equal 1.5 the length of embedded part of the pile. These arrangements will display the soil behavior without creating any stress concentration on the mesh's boundaries.

In the present investigation, a predefined hole will be placed in the soil to simulate uplift behavior for already driven piles in the ground.

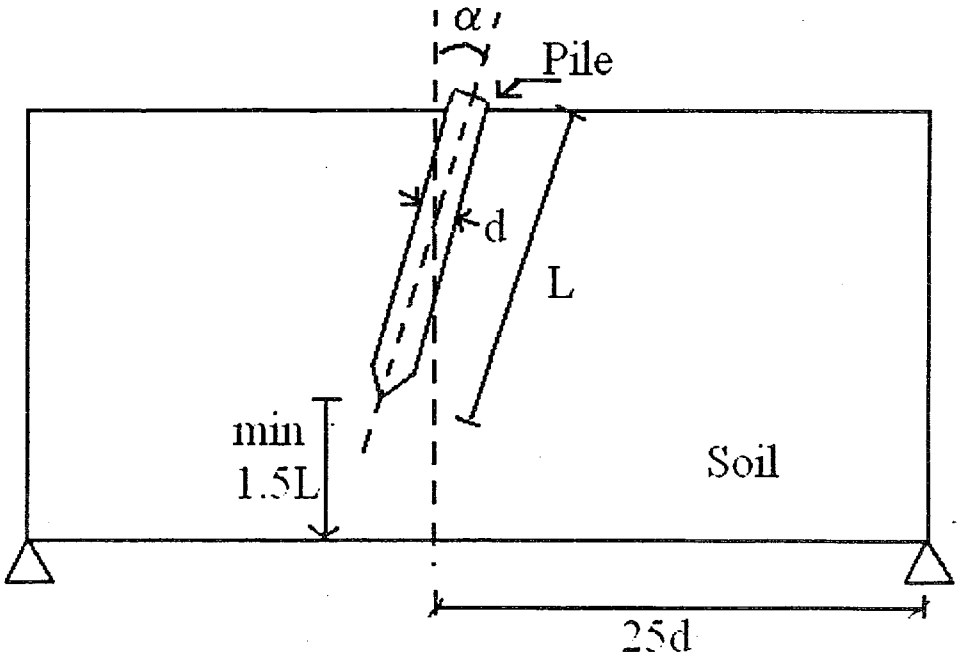

Figure 3. 5 Suggested Soil Dimensions after Randolph (1977)

Figure 3. 6 presents the 3D model developed in this investigation. As shown in this figure, elements at the bottom of the mesh were treated as fixed in both vertical and horizontal directions, while, the vertical boundaries were constrained in the horizontal direction.

There could be two application procedures to determine failure stress in soil. One is to apply a force on top of the pile and measure the failure stress according to load-displacement curve, second is to assign a displacement value upward and measure the failure stress. Both principles have given same results in this particular model.

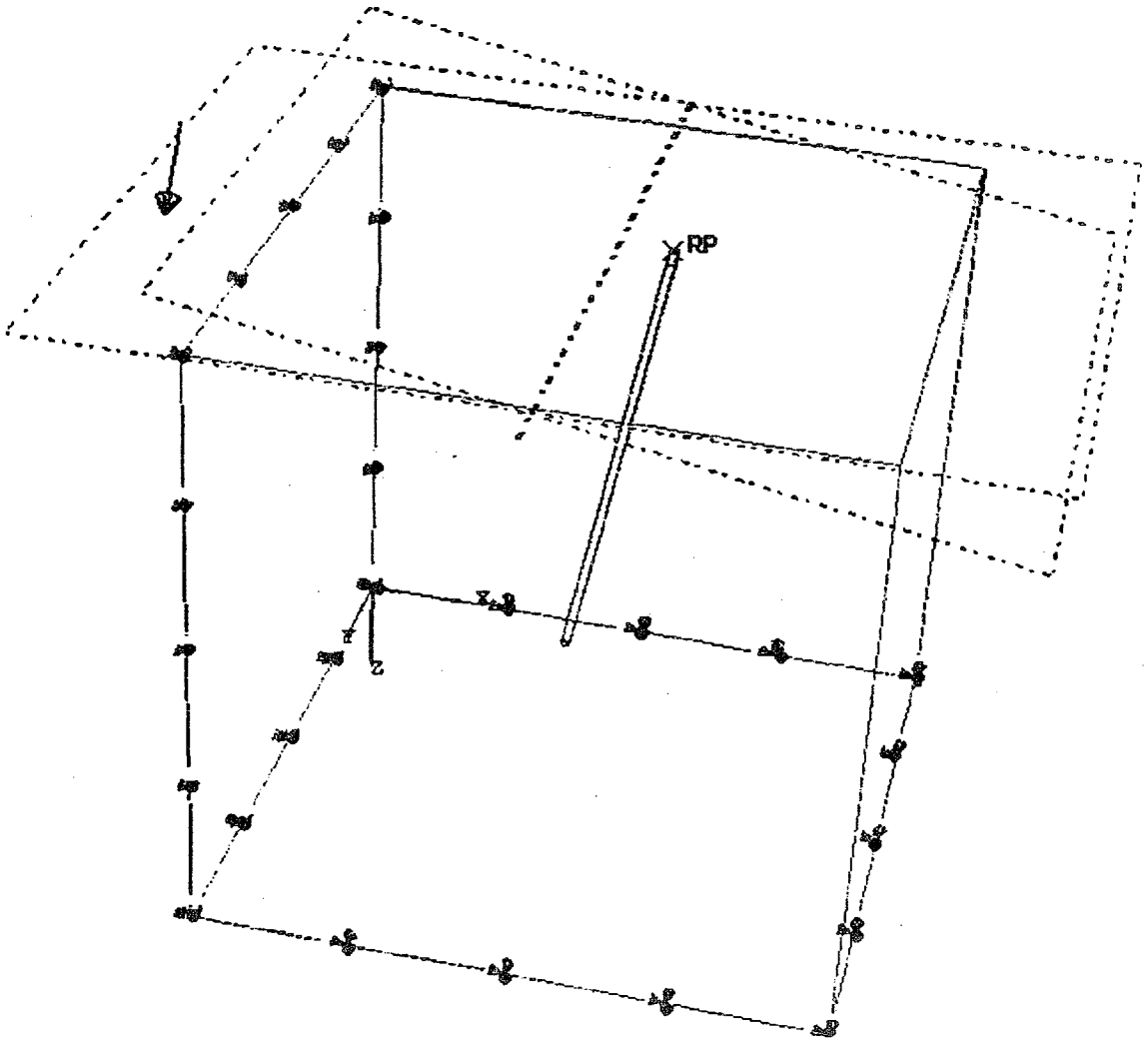

Figure 3. 6 Boundary Conditions of Initial Stage-Present Study

As seen in Figure 3. 6, assembly is a space where boundary conditions, instances, load application, datum planes, and angles are applied. Therefore for each model having different angle, dimensions, and boundary conditions will be a unique assembly. To create an inclined pile one must have an inclined hole.

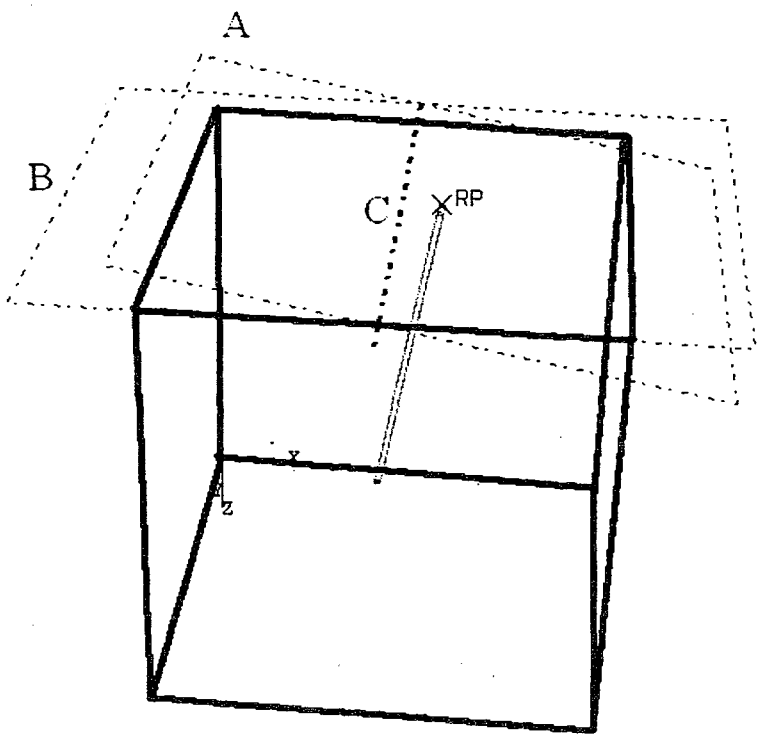

Figure 3. 7 Assembly of Soil and Pile-Present Study

Figure 3. 7 illustrates the datum plane B parallel to part surface where a pile hole will punch through the soil. In order to install a battered pile, another datum plane was created with an angle option to datum plane B. To assign turning axis datum c axis should be created. This will allow the user to create a hole at the desired angle

3.2.3 Soil constitutive model

In this investigation, the constitutive model of Mohr-Coulomb will be used to model soil behavior, as follow:

$$\tau = c + \sigma \tan \delta \qquad (3.1)$$

Where:

τ: Shear stress

c: Soil Cohesion

δ: Interface angle

Mohr-Coulomb theory allows the material to harden or soften isotropically. The elastic part of the response is specified in elastic (Hook) theory. For the hardening behavior of the material, isotropic cohesion hardening is assumed according to strain-stress values of particular soil.

Table 3. 1: Sample Trial values for Mohr-Coulomb plastic model for 38 mm pile

Parameter	Unit	Sample Trial Value
Friction Angle	Degree	39
Dilatation angle	Degree	10
Meridian Eccentricity	n/a (ratio)	0.1
Soil Dimension	Feet	3.1
Pile Diameter	Feet	0.124
L/D	n/a (ratio)	40
Unit Weight	N/ft^3	515.43

It is important to note that since ABAQUS is dimensionless[2]. Parameter-units must be in the same standard system. A trial sample values were demonstrated in Table 3. 1.

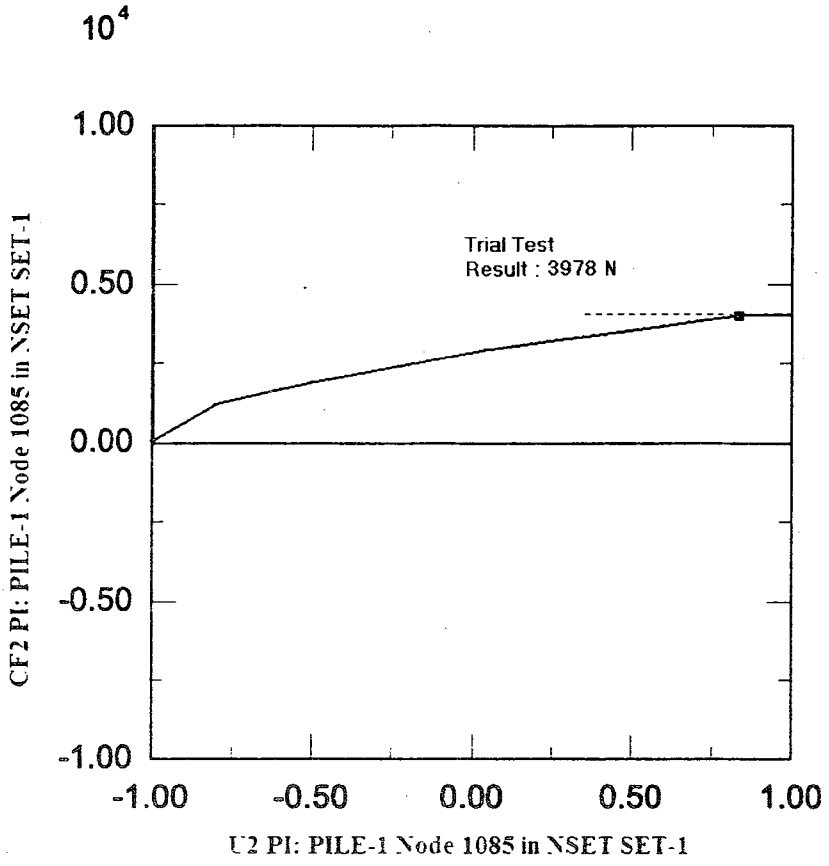

Figure 3. 8 Typical Output Trial Test Values

Figure 3.8 shows a trial test on model where x and y axis are "Applied Load" and "Displacement in Load Direction" respectively. During the analysis, the program recommends to reduce or increase some of the properties of tet-shape (TS) meshed elements. TS elements are meshed by free meshing procedure. Although it is free-meshing, some restrictions can be applied.

[2] Some parameters have assigned-units. Ex: Angle is in degrees. See ABAQUS manual for details.

Shape factor: 0.0001

Face corner angle less than: 5

Face corner angle: 170

Aspect ratio greater than: 10

Edge shorter than: 0.01

Seeding of parts will define the maximum element size and the value will assign the number of nodes on the edges. This value was taken as 1.5 (according to Hanna & Afram 1986). This was mainly due to the fact that trials showed that meshing finer (using smaller values) did not change ultimate capacity significantly.

3.2.4 Interaction between Pile and Soil Surface

The program allows the user to select different interaction properties including: surface to surface, self-surface or acoustic impedance. The present case will be best be represented by surface to surface solution.

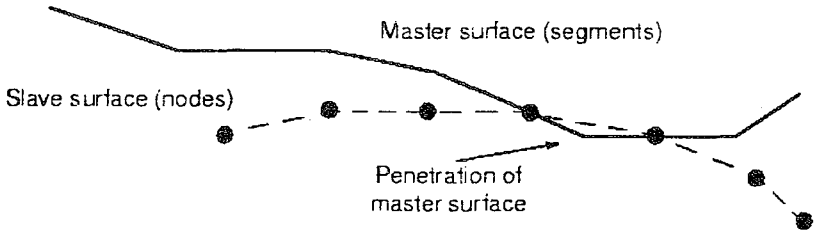

Figure 3. 9 Master & Slave surface interaction-ABAQUS Manual (2006)

An extended version of the classical isotropic friction model is provided in for use with all contact analysis capabilities. The extensions include an additional limit on the allowable shear stress, anisotropy, and the definition of a "secant" friction coefficient.

The standard friction model assumes that no relative motion occurs if the equivalent frictional stress, τ_{eq} is less than the critical stress, τ_{cr}

$$\tau_{eq} = \sqrt{\tau_1^{\,2} + \tau_2^{\,2}} < \tau_{cr} \tag{3.2}$$

Which is proportional to the contact pressure, p;

$$\tau_{cr} = \mu p \tag{3.3}$$

where μ is the frictional coefficient that can be defined as the function of the contact pressure, p; the slip rate, γ_{eq}; the average surface temperature at the contact point; and the average field variables at the contact point. Rate-dependent friction cannot be used in a static Riks analysis since velocity is not defined. In this model it is possible to put a limit on the critical stress:

$$\tau_{cr} = \min(\mu p, \tau \max) \tag{3.4}$$

where $\tau_{\max}$ is user-specified. If the friction is isotropic, the direction of the slip and the frictional stress coincide, which is expressed in the form

$$\frac{\tau_i}{\tau_{eq}} = \frac{\gamma_i}{\gamma_{eq}} \tag{3.5}$$

where γ_i is the slip rate in direction i and γ_{eq} is the magnitude of the slip velocity,

$$\gamma_{eq} = \sqrt{\gamma_1^{\,2} + \gamma_2^{\,2}} \tag{3.6}$$

The stiffness is chosen such that the relative motion from the position of zero shear stress is chosen by a value of γ_{cr}. The critical slip value γ_{cr} is specified to 0.5% of the average length of all contact elements in the model. With the penalty contact algorithm the relative motion in the absence of slip is equal to the friction force divided by the penalty stiffness. The interaction therefore requires following assumptions.

- At the beginning of the analysis nodes from two part (soil and pile) are in contact
- As shown in Figure 3.9, nodes on the slave surface (soil) cannot penetrate the segments that make up the master surface (pile)
- Small-Sliding is accepted for this model. The finite-sliding contact formulation requires program constantly determines which part of the master surface is in contact with each slave node. Note, this is a very complex calculation, and computationally expensive. When the contacting bodies are both deformable the solution will be unreliable.
- Pile & Soil interaction was selected as tangential, isotropic behavior, as friction method penalty method was used. Helwany (2007) used friction coefficient between 0.1 and 0.3 for sand-modeled soil where water was not present.

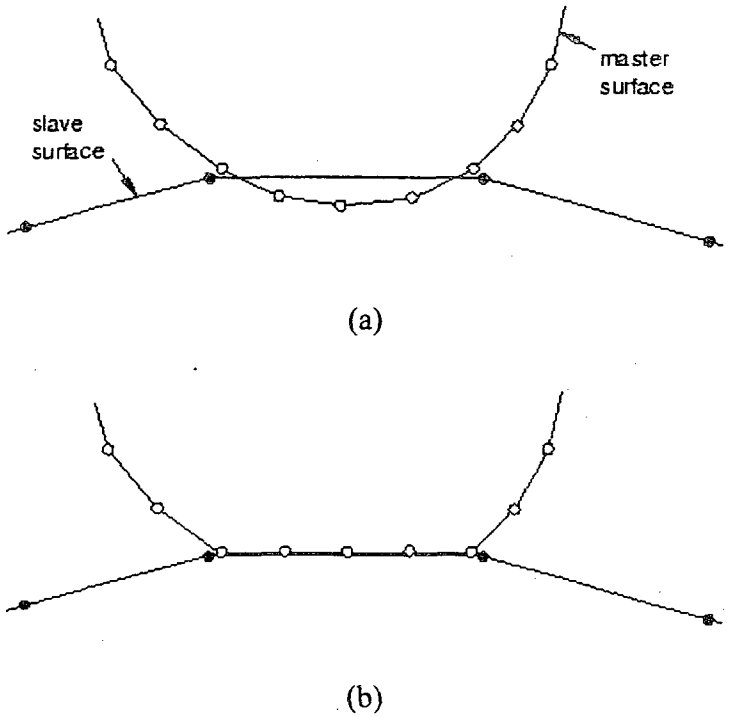

Figure 3. 10 Master & Slave surface adjustment (a&b) -ABAQUS Manual (2006)

Interaction of pile and soil surface can also be controlled with some elements. The results of the trials have shown that adjusting nodes as seen on Figure 3.10 (b) will alter work-done throughout friction analysis. This will affect pressure transferred from nodes-to-nodes and hence it increases the ultimate pile capacity. Consequently adjusting nodes at the beginning of the analysis as seen in Figure 3.10 (b) is not used to represent in-situ interaction for predefined (bored) holes. Adjustment of nodes should be considered for driven piles.

3.2.5 Validation of Model & Test Procedure

Results generated by the program are somewhat hard to read as compared to other software mostly designed for geotechnical applications. Therefore load-displacement curves are designed to read stress states and failure pattern.

According to facilitate reading the output, these assumptions were made:

- Failure generally starts at a point closer to the tip of the pile. To be more precise, from the tip of the pile approximately 5d-zone and less, depending on the inclination.
- $K_i = K_o$ state is accepted due to the initial conditions of pile hole.
- Gravity applied to the system creates a small eccentricity due to inclination of pile hole. The effect of inclination is neglected because it creates less than 5-10% (from 10^o to 45^o) error in comparison with available experimental data on overall ultimate pile capacity for the maximum 45^o inclination.
- Failure takes place where Load-Displacement curve tends to be straight or with a degree close to the horizontal direction.

Model Validation

The results obtained by the present numerical model were compared with the following laboratory and field data:

1. Laboratory results of Hanna & Afram for pullout

2. Tension or Compression loads

3. Real pile pullout tests

Load-Displacement curves are used to read failure mechanism. It is seen that from certain point, increase in displacement with invariant load, interaction of pile & soil reaches failure.

As mentioned above the program drives user to define certain units because of its dimensionless nature. A typical input must be in the same unit system. Outputs are presented in Figure 3.11.

Table 3. 2: Typical input values of test model A-1

Test	L	D	ϕ	α (inclination)	Unit Weight	Pile Capacity
No	(feet)	(feet)	Degree	Degree	N/ft3	N
A-1	5.08	0.124	39	0	442.082239	1535

Seeding ratio: 1.5
Shape factor: 0.0001
Face corner angle less than: 5
Face corner angle: 170
Friction Coefficient μ=0.1
Aspect ratio greater than: 10
Edge shorter than: 0.01
Dilatation angle ψ: 25
Plain Stress/Strain Thickness: 1
Fraction Characteristics of Surface Dimension: 0.1

Table 3. 3: Comparison between Present Study and Test Results of Hanna & Afram, 1986 (38 mm)

Test No	L (mm)	D (mm)	ϕ Degree	α (inclination) Degree	Unit Weight kN/m3	Pile Capacity N	Present Study N
A-1	1549	38	39	0	15,6	1535	1524
A-2	1549	38	39	10	15,6	1526	1530
A-3	1549	38	39	20	15,6	1517	1539
A-4	1549	38	39	30	15,6	1512	1551

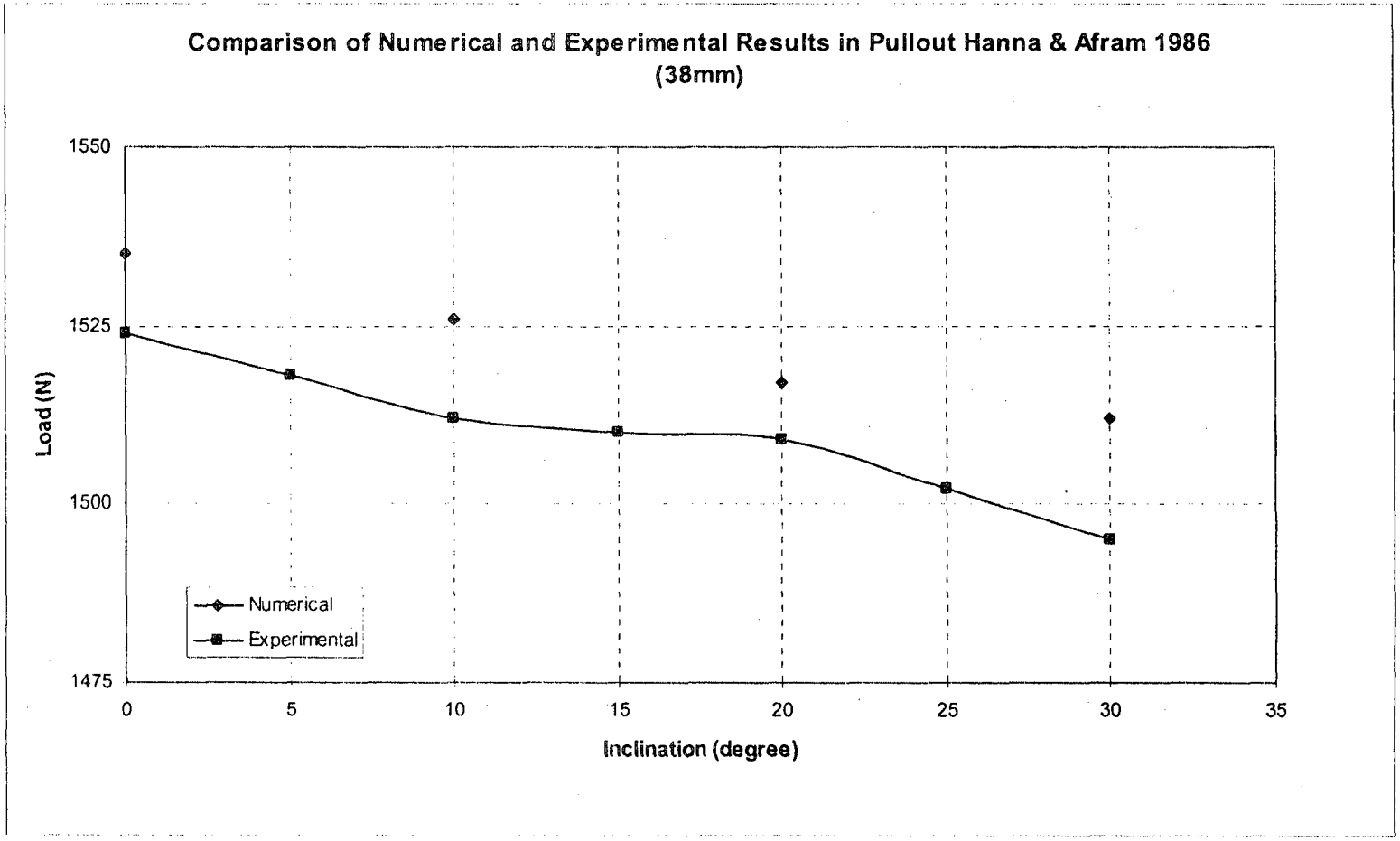

Figure 3. 11 Comparison of Numerical and Experimental Results in Pullout

Figure 3.11 indicates that results obtained from numerical analysis shows resemblance to laboratory results. As seen in the Figure 3.12, between 10 and 20 degrees shaft resistance slightly decreases as the angle increases.

Table 3. 4 Comparison of Present Study with Test Results of Hanna & Afram, 1986 (76mm)

Test No	L (mm)	D (mm)	ϕ Degree	α (inclination) Degree	Unit Weight kN/m3	Pile Capacity N	Present Study N
A-5	1549	76	39	0	15,6	3536	3534
A-6	1549	76	39	15	15,6	3501	3548
A-7	1549	76	39	30	15,6	3430	3610

Figure 3.11 illustrates that when pile diameter is increased results comply with experimental results. However, pile capacity comparison with experimental results becomes more flawed with respect to inclination of pile considering experimental results are more accurate.

The phenomenon can be explained by the application of gravity force. As mentioned earlier, gravity on 3D model creates an eccentricity that will lead less accurate results with large-size piles because of the stress accumulated on membrane of pile-soil interaction.

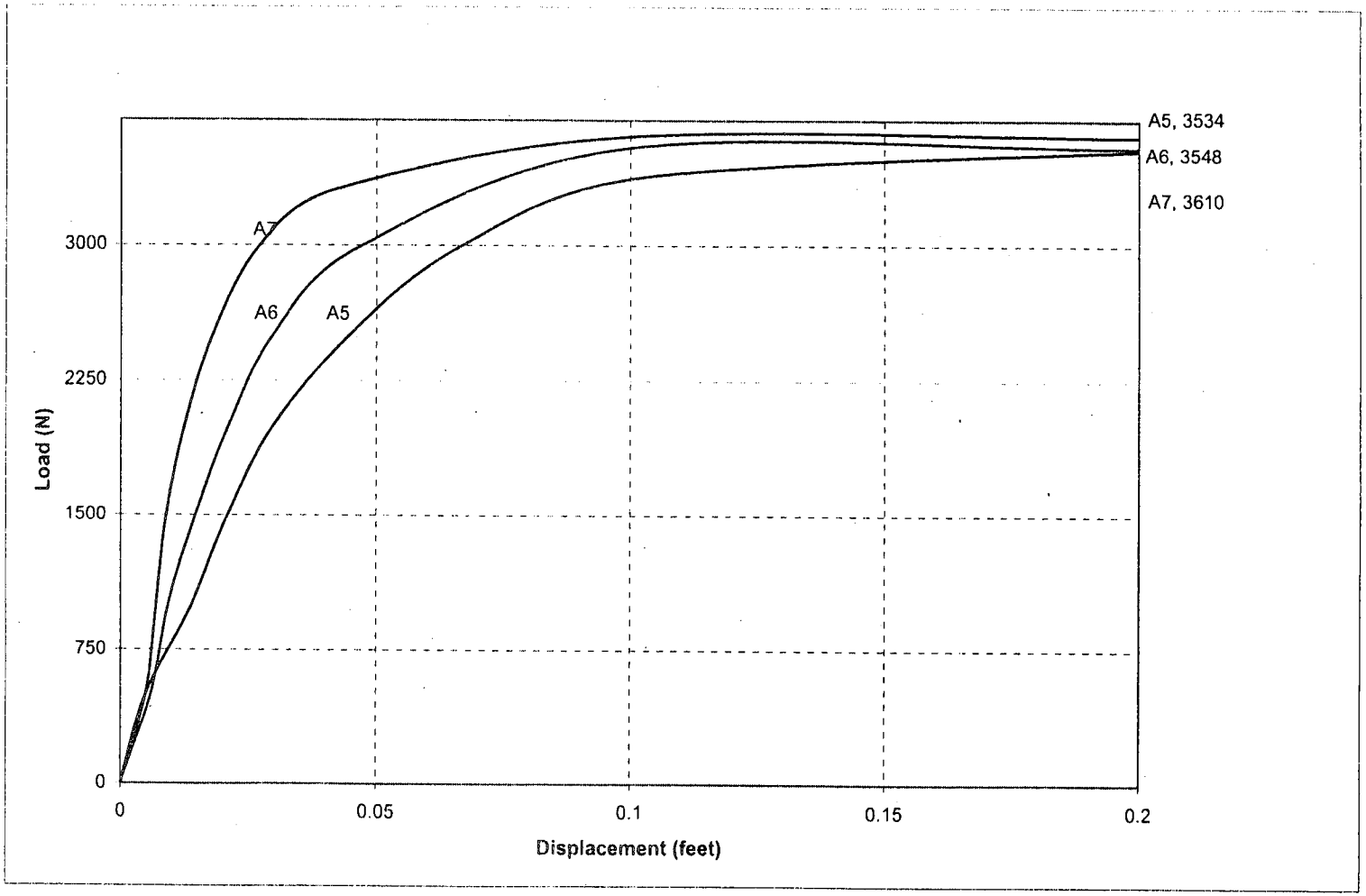

Figure 3. 12 Numerical Results of A5 to A7, Compared Model to Hanna & Afram Test Results (1986)

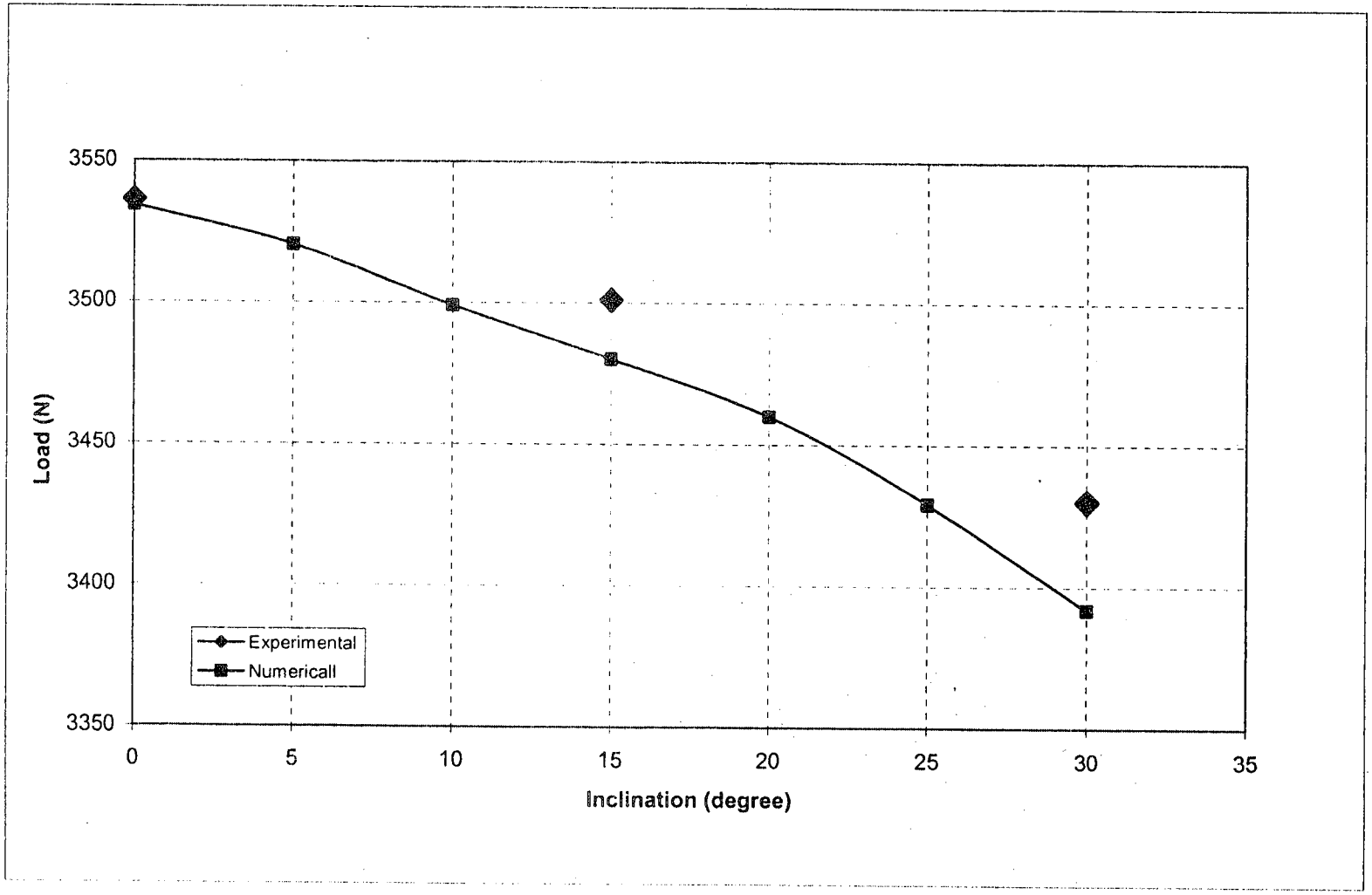

Figure 3. 13 Comparisons of Numerical and Experimental Results in Pullout 76mm- Hanna & Afram (1986)

Table 3. 5 Comparison of Present Study with Hanna &Nguyen, 2003(38mm) Compression $\alpha=0^{o}$

Test No	D (mm)	L/D (dimensionless)	ϕ Degree	α (inclination) Degree	Unit Weight kN/m3	Pile Capacity N	Present Study N
B-1	38	10	39	0	18,2	600	589
B-2	38	20	39	0	18,2	1640	1645
B-3	38	30	39	0	18,2	3430	3050
B-4	38	40	39	0	18,2	4159	4050

As seen in Figure 3.12 results from numerical study with vertically driven piles act in accordance with experimental studies. However, when the inclination increases as seen in Figure 3.13, shaft resistance values from numerical studies are not comparable the experimental studies tolerably. The error band is from 15 to 27 % of the experimental value.

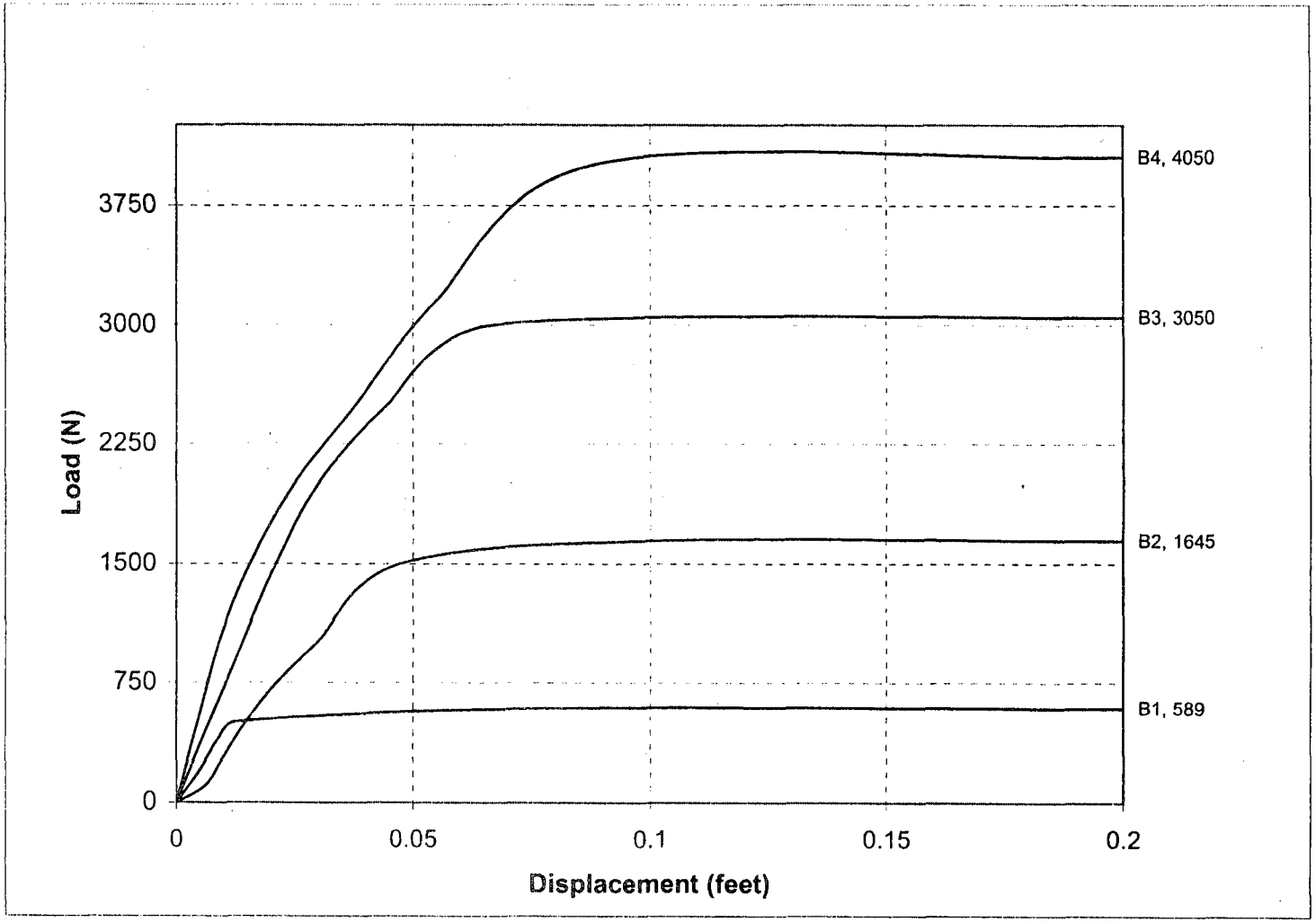

Figure 3. 14 Numerical Results of B1 to B4, Compared Model to Hanna & Nguyen Test Results 2003

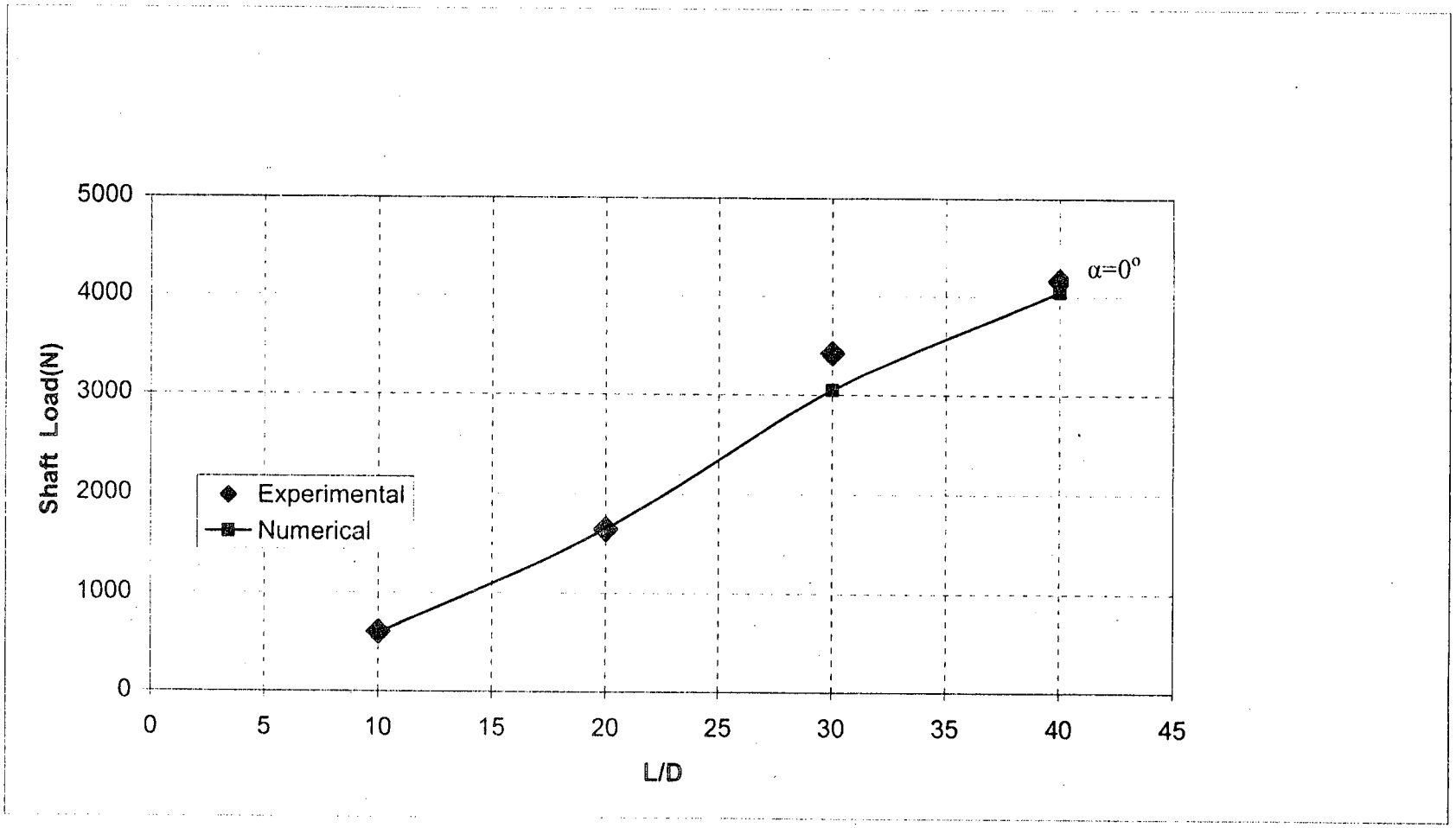

Figure 3. 15 Comparisons of Numerical and Experimental Results in Pullout 38mm-Hanna & Nguyen (2003)

Table 3. 6 Comparison of Present Study with Hanna &Nguyen, 2003 (76mm) Compression $\alpha=10^{o}$

Test No	D (mm)	L/D (dimensionless)	ϕ Degree	α (inclination) Degree	Unit Weight kN/m3	Pile Capacity N	Present Study N
B-5	76	5	39	10	18,2	610	450
B-6	76	10	39	10	18,2	2082	1962
B-7	76	15	39	10	18,2	3825	3050
B-8	76	20	39	10	18,2	5867	5003

As seen in Figure 3.15, when L/D reaches between 25-30 in value slopes changes slightly. Although an argument has been previously mentioned about the variation of experimental and numerical results for compression loading this could be critical region for L/D because the comparison-in fact-starts to vary from this region forward. This difference is more visible as the inclination angle increases. Truly, with more comparison values a more definite picture can be drawn.

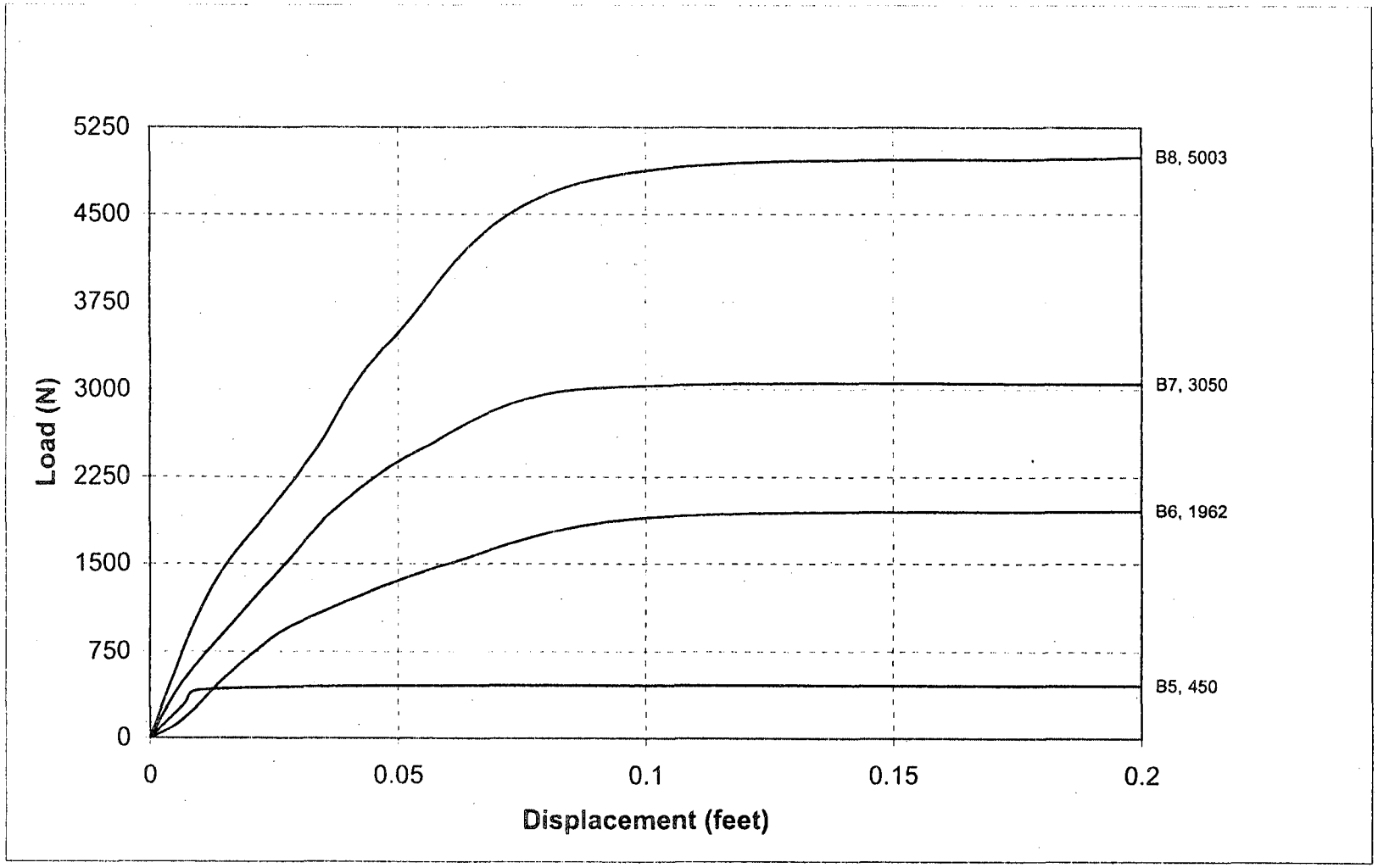

Figure 3. 16 Numerical Results of B5 to B8, Compared Model to Hanna & Nguyen Test Results (2003)

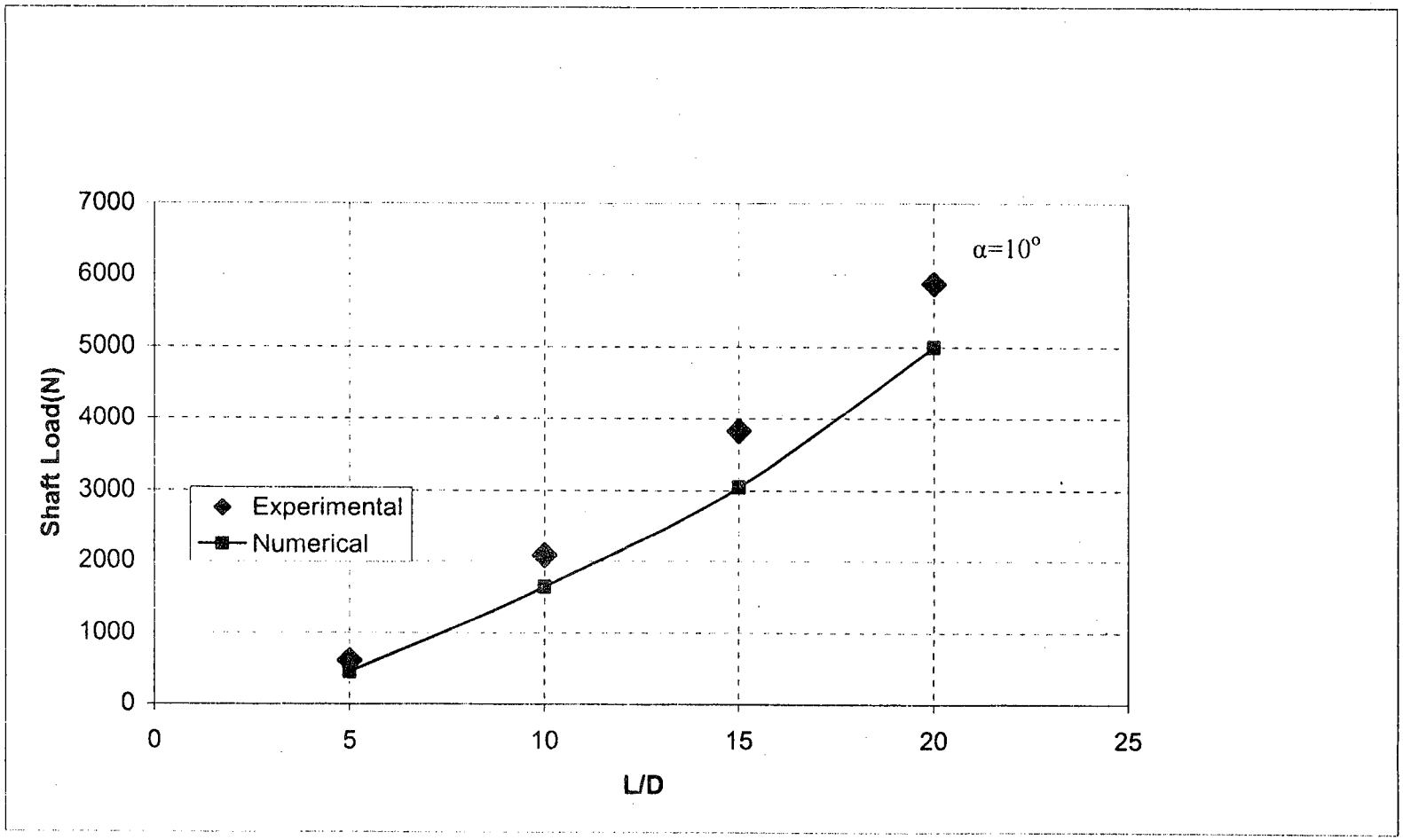

Figure 3. 17: Comparisons of Numerical and Experimental Results in Pullout 76mm-Hanna & Nguyen (2003)

Table 3. 7 Comparison of Present Study with Hanna &Nguyen, 2003 (38mm) Compression α=20°

Test No	D (mm)	L/D (dimensionless)	ϕ Degree	α (inclination) Degree	Unit Weight kN/m3	Pile Capacity N	Present Study N
B-9	38	10	39	20	18,2	461	445
B-10	38	20	39	20	18,2	1253	1080
B-11	38	30	39	20	18,2	2456	2150
B-12	38	40	39	20	18,2	3850	3300

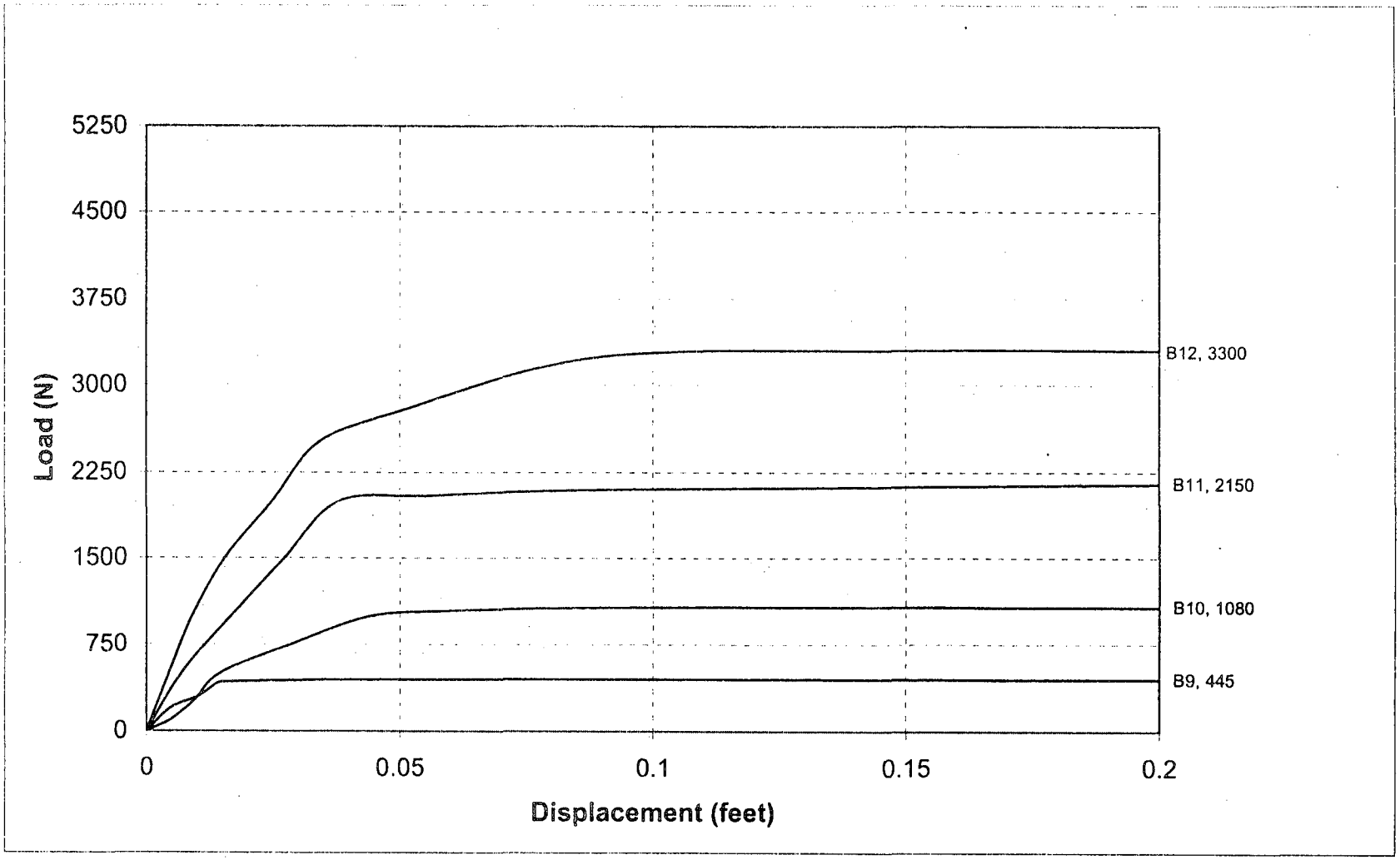

Figure 3. 18 Numerical Results of B9 to B12

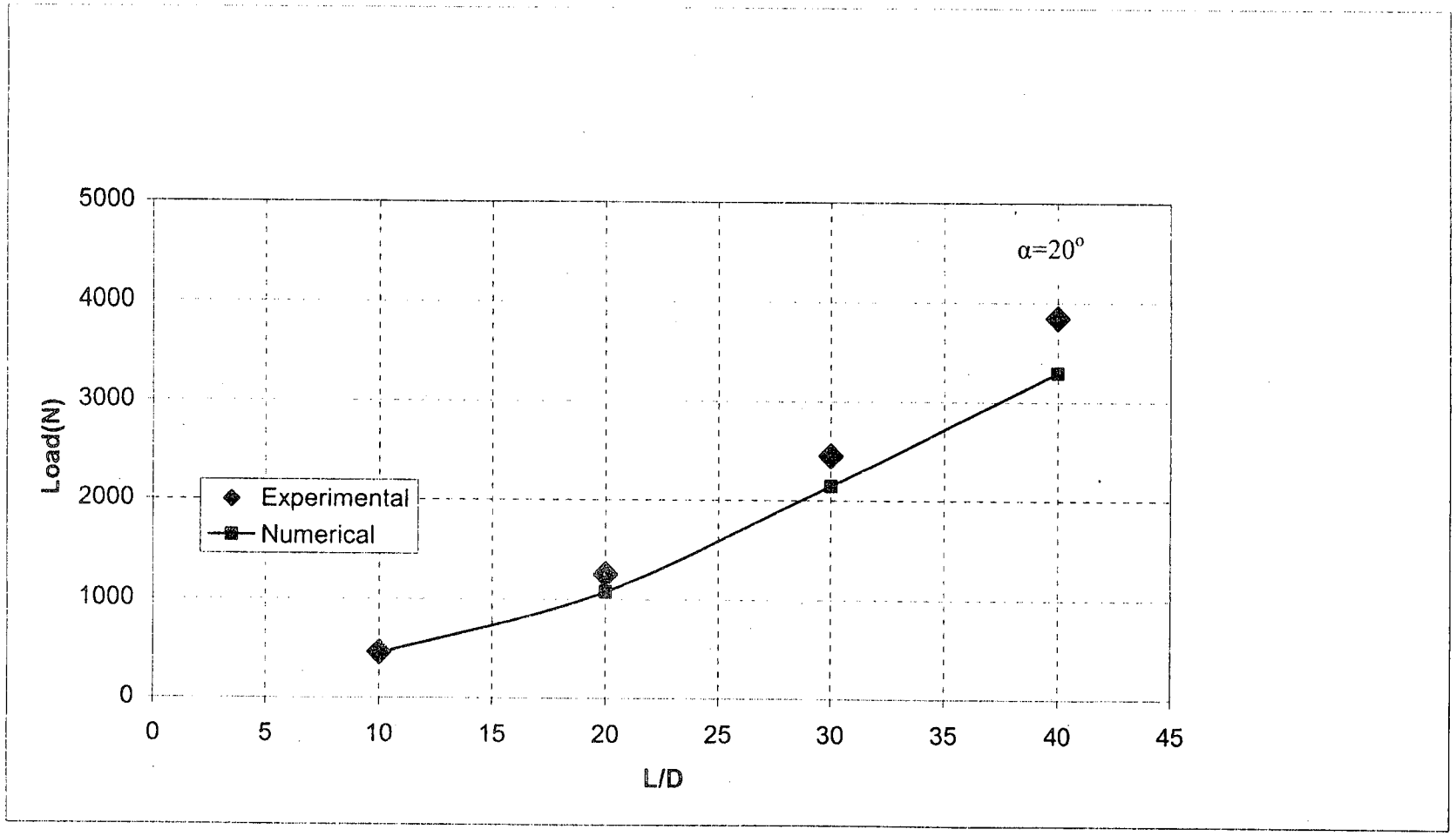

Figure 3. 19 Comparison of Numerical and Experimental Results in Pullout 38mm-Hanna & Nguyen (2003)

Table 3. 8 Comparison of Present Study with Alewnah 1999, $\alpha=0^{o}$

Test No	D (mm)	L/D (dimensionless)	ϕ Degree	α (inclination) Degree	Unit Weight kN/m3	Pile Capacity kN	Present Study kN
C-1	0,46	25,25	37	0	12,3	1128	1178
C-2	0,46	29,8	37	0	11,9	1300	1288

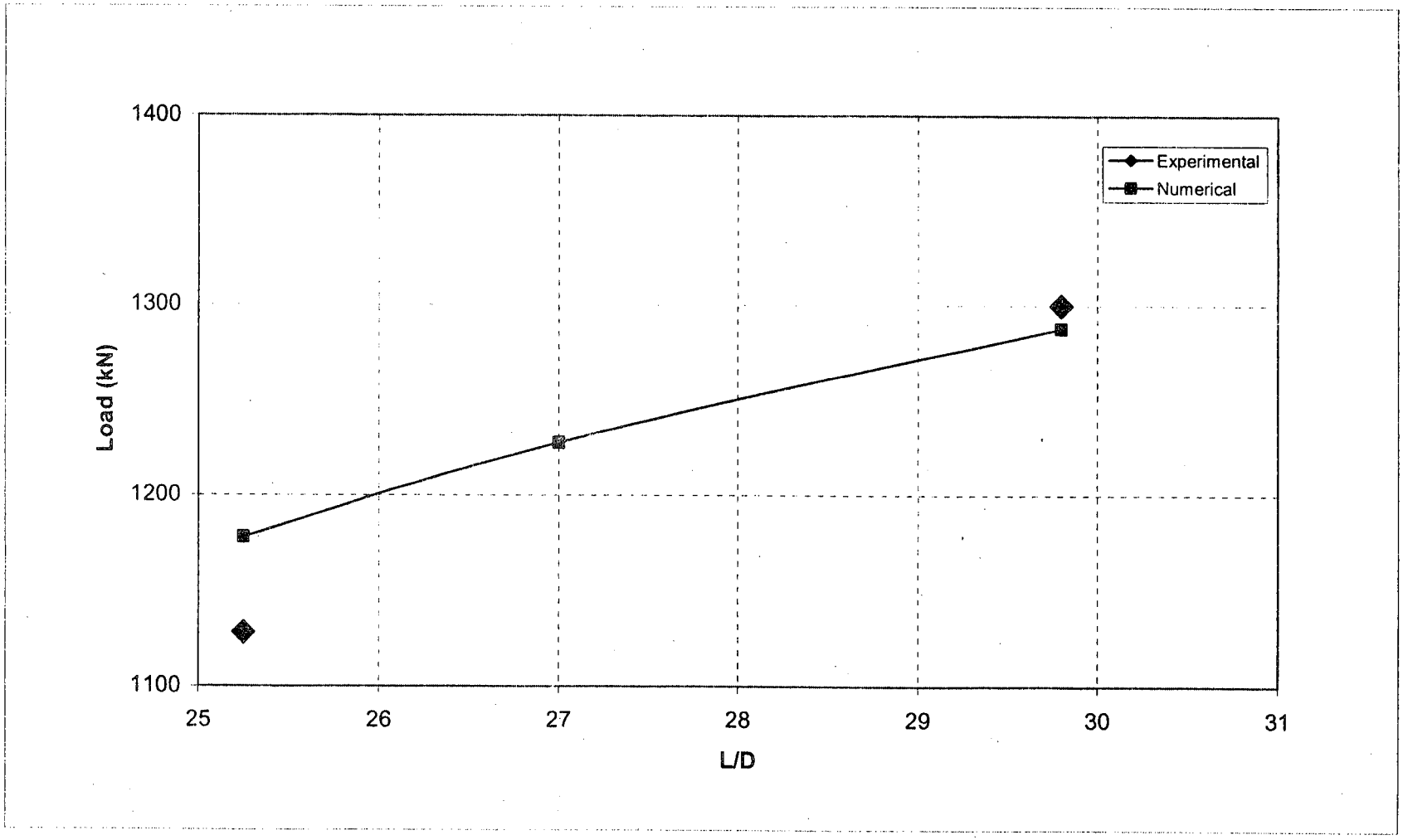

Figure 3. 20 Tension in-situ Test Results $\alpha=0^{\circ}$ of Jonesville Lock and Dam Sherman et al. (1999)

The presented data (Table 3.8) is obtained from closed-ended real concrete pile test results partially submerged to water.

According to the results obtained from numerical analysis, it can be safely said that 3D model is reliable for tension, and vertical compression piles. Using additional examples design charts are presented in next title.

3.3 TEST RESULTS & ANALYSIS

3.3.1 Effect of Pile Length & Diameter

It is a universal fact that with the increase of length shaft resistance increase due to overburden pressure creating horizontal pressure. Although it is expected that shaft resistance will show general ascent, from certain point this rate decreases with respect to density, pile length, pile diameter, and driving technique. This phenomenon is called "critical depth". Randolph et al (1993) found that for vertical piles critical depth point is within 10-20 L/D in cohesionless soil.

Figure 3.22 and Figure 3.23 clearly indicates that a critical depth is present between the depth/diameter ratios of 15-20.

Table 3. 9 Critical L/D values in compression

	L(m)	D(m)	Critical Depth (L/D)	Sand Type
Mansour & Kaufman 1956	19.8	0.53	15-20	Dense
Beringen et al 1979	6.7	0.36	16-18	Very Dense

Figure 3.21 presents numerical values from current study in tension loading. It should be noted that for critical depth zone shaft resistance can drop drastically from 10 to 40 %.

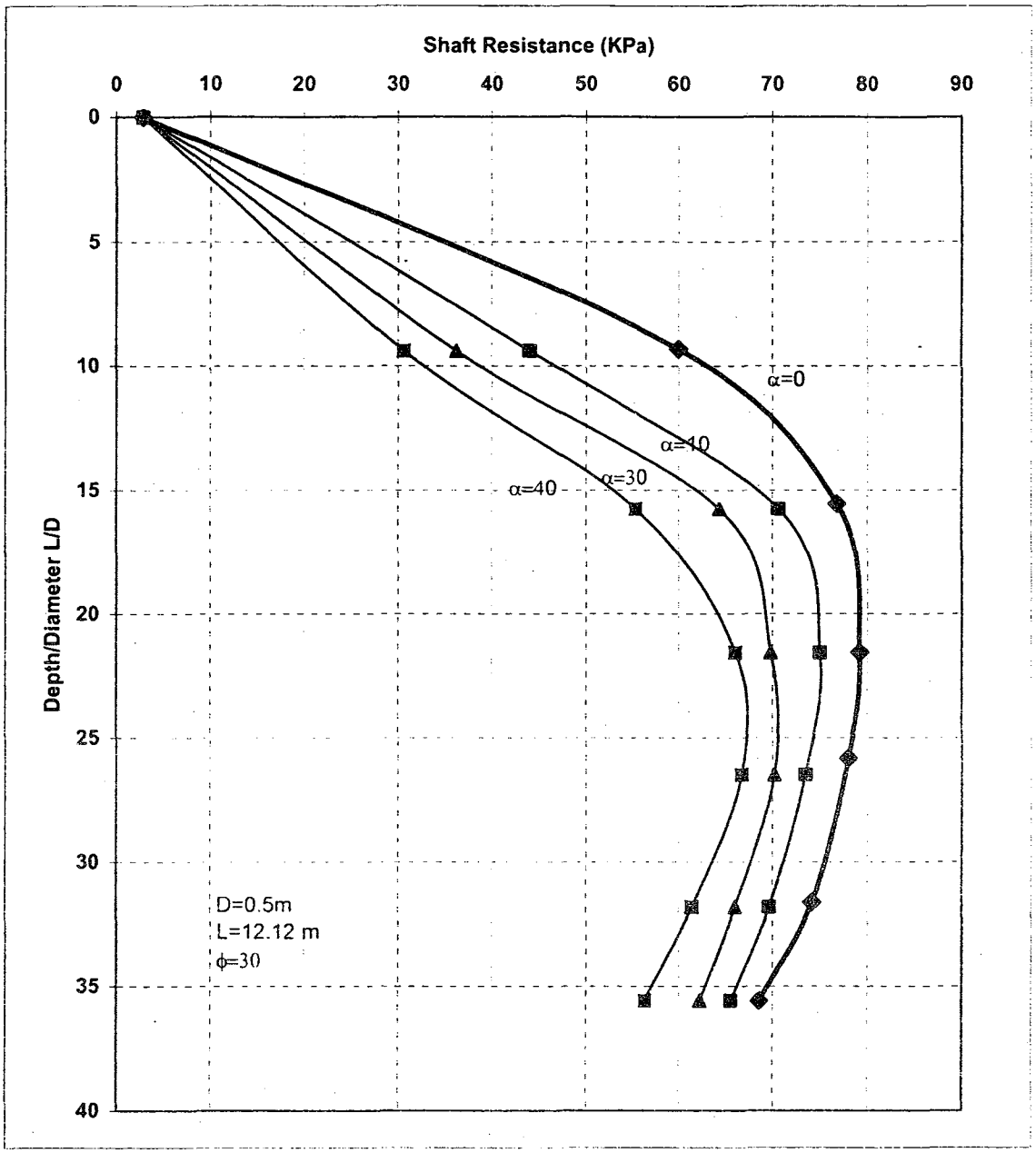

Figure 3. 21 Shaft resistance of in tension for different inclinations-Present study

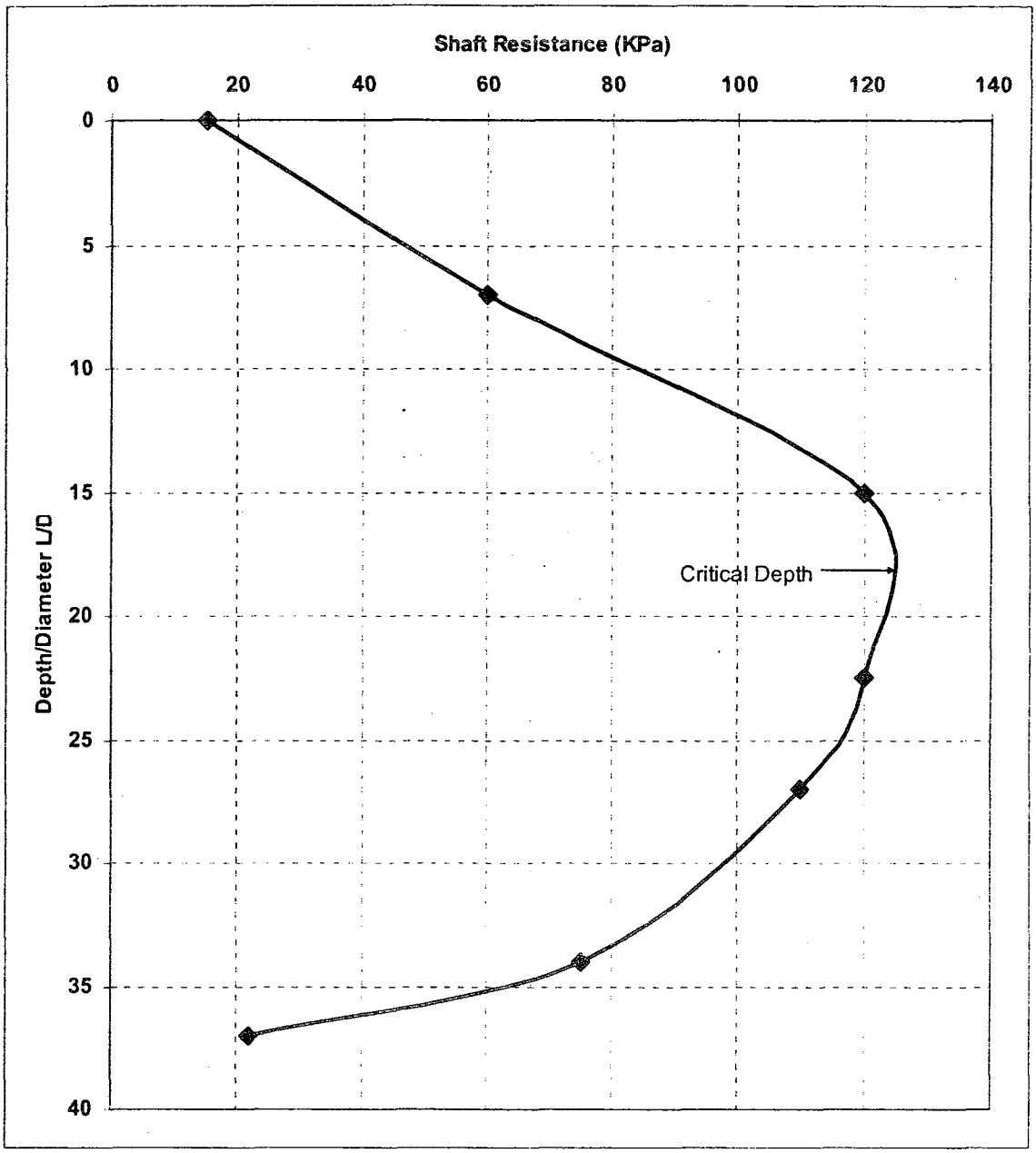

Figure 3. 22 Shaft resistance of a compression test in sand after Mansour& Kaufman (1956)

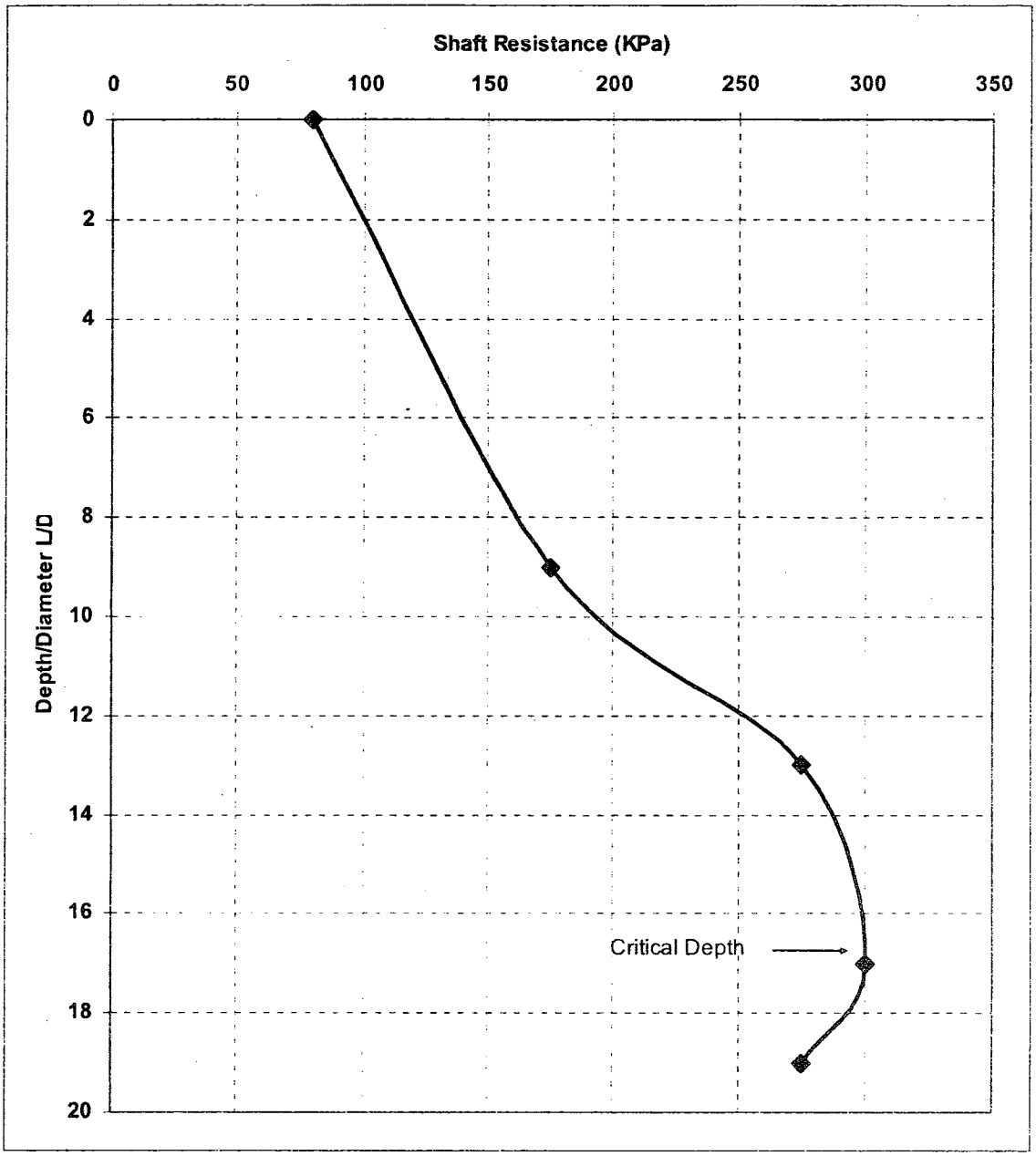

Figure 3. 23 Shaft resistance of a compression test in sand after Beringen et al (1979)

3.3.2 Effect of inclination angle

Considering inclination purposes, effect of inclination in batter piles is evident. However, for certain degree as presented on Figure 3.24, the coefficient of earth pressure affecting shaft resistance predominantly has approximate equal values despite there are slight differences between angles. According to Hanna & Nguyen (1986) study shaft resistance decreases with the increase of inclination, while Meyerhof (1973) claims the opposite. Another study by Hanna & Afram (1986) shows there is no significant change in shaft resistance with the increase of inclination.

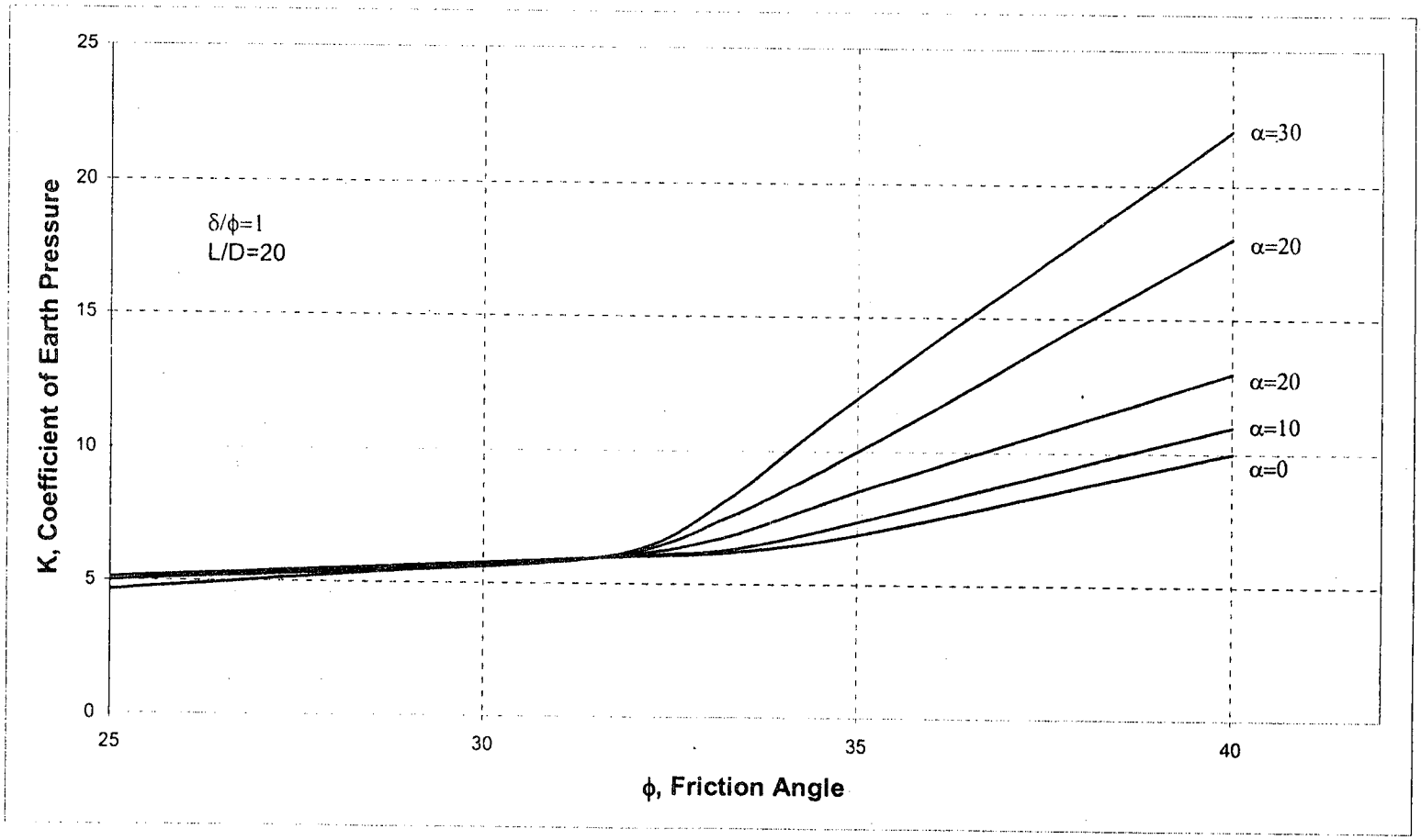

Figure 3. 24 Friction angle vs. K values in respect to inclination angles-Present Study

Table 3. 10 Batter Piles subjected to Pullout in Sand Test results of Hanna & Afram (1986)

Pile Diameter D(mm)	Angle of Inclination α	Pullout Load (N)	Weight of the Pile (N)
38	0	1535	69
38	10	1526	69
38	20	1517	69
38	30	1512	69
76	0	3536	162
76	15	3501	162
76	30	3430	162

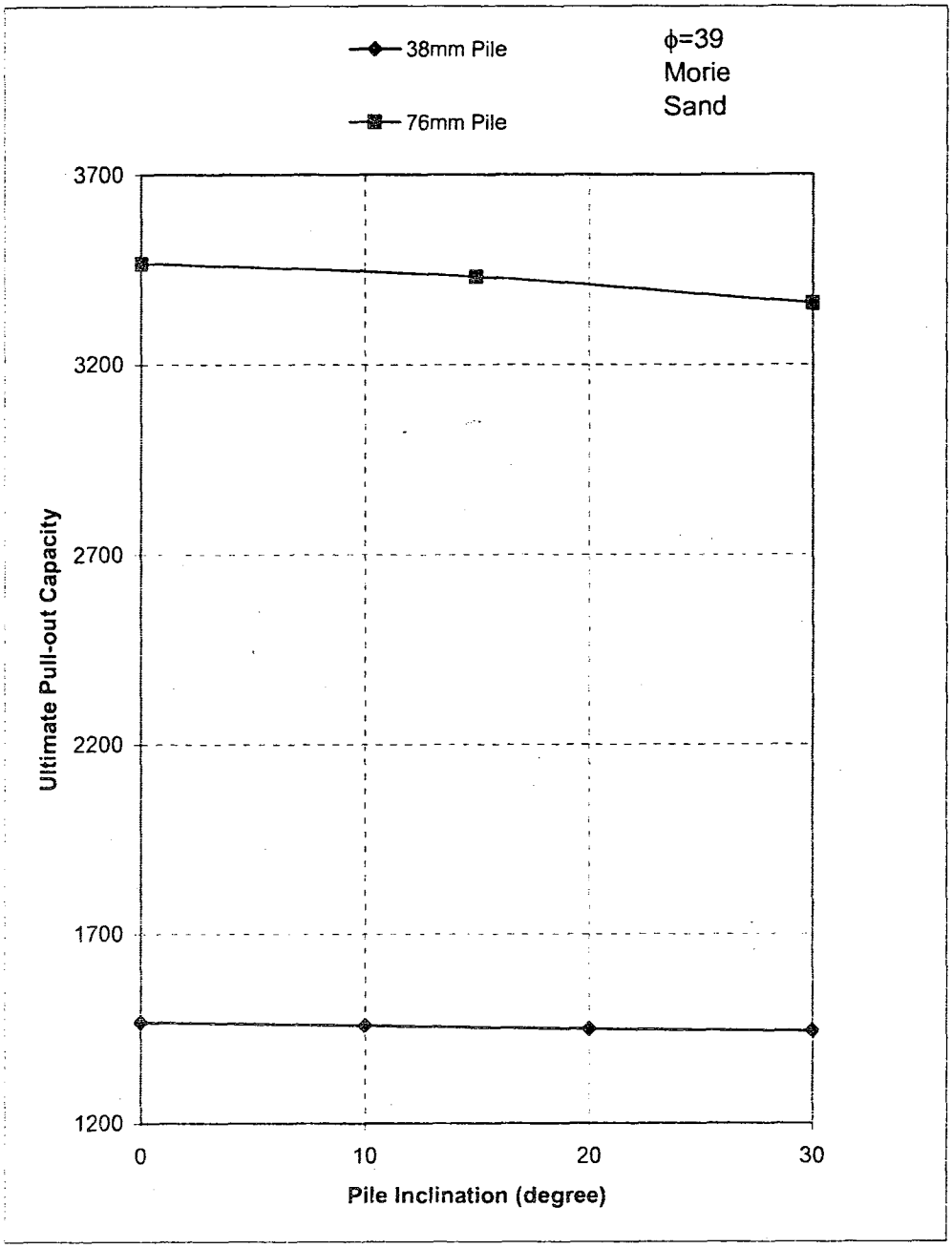

Figure 3. 25 Ultimate Pull-out Capacity vs Pile Inclination after Hanna & Afram (1986)

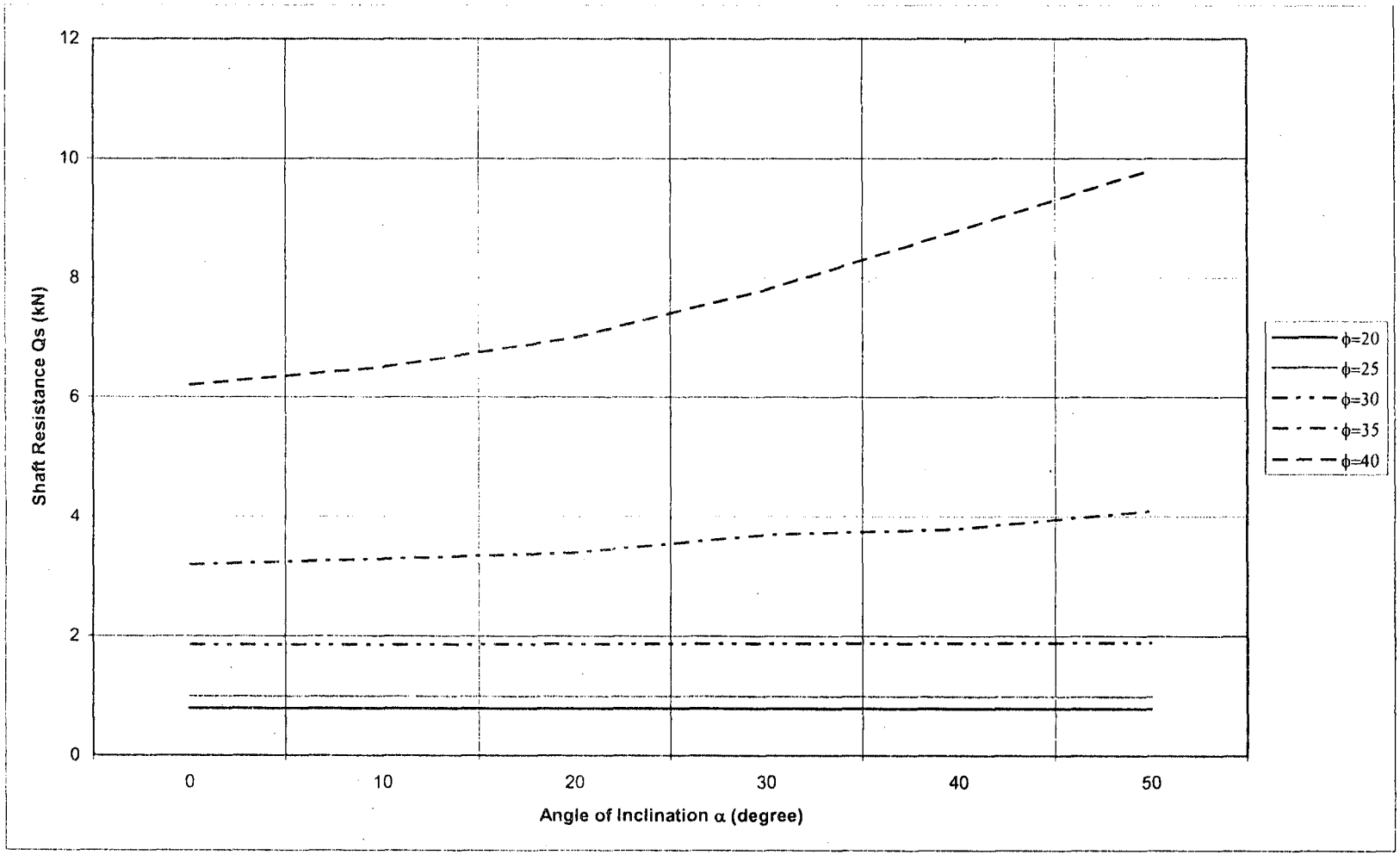

Figure 3. 26 Shaft Resistance vs Pile Inclination after Sabry (2001)

CHAPTER IV

THEORETICAL APPROACH & DESIGN PROCEDURE

4.1.GENERAL

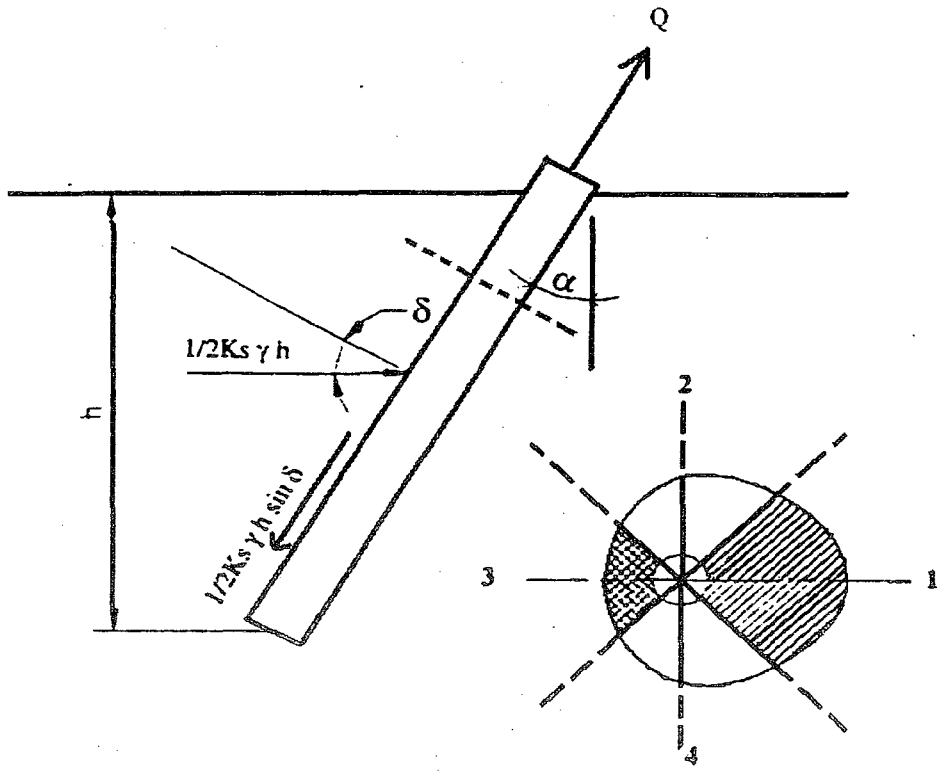

Figure 4. 1 Force Equilibrium under pullout

Figure 4.1 shows here distribution of pressure for a pile under tension loading with inclination α degree. This is a general presumption of pressure distribution around the pile to solve equation. However, it is apparently accurate as demonstrated in Figure 4.2.

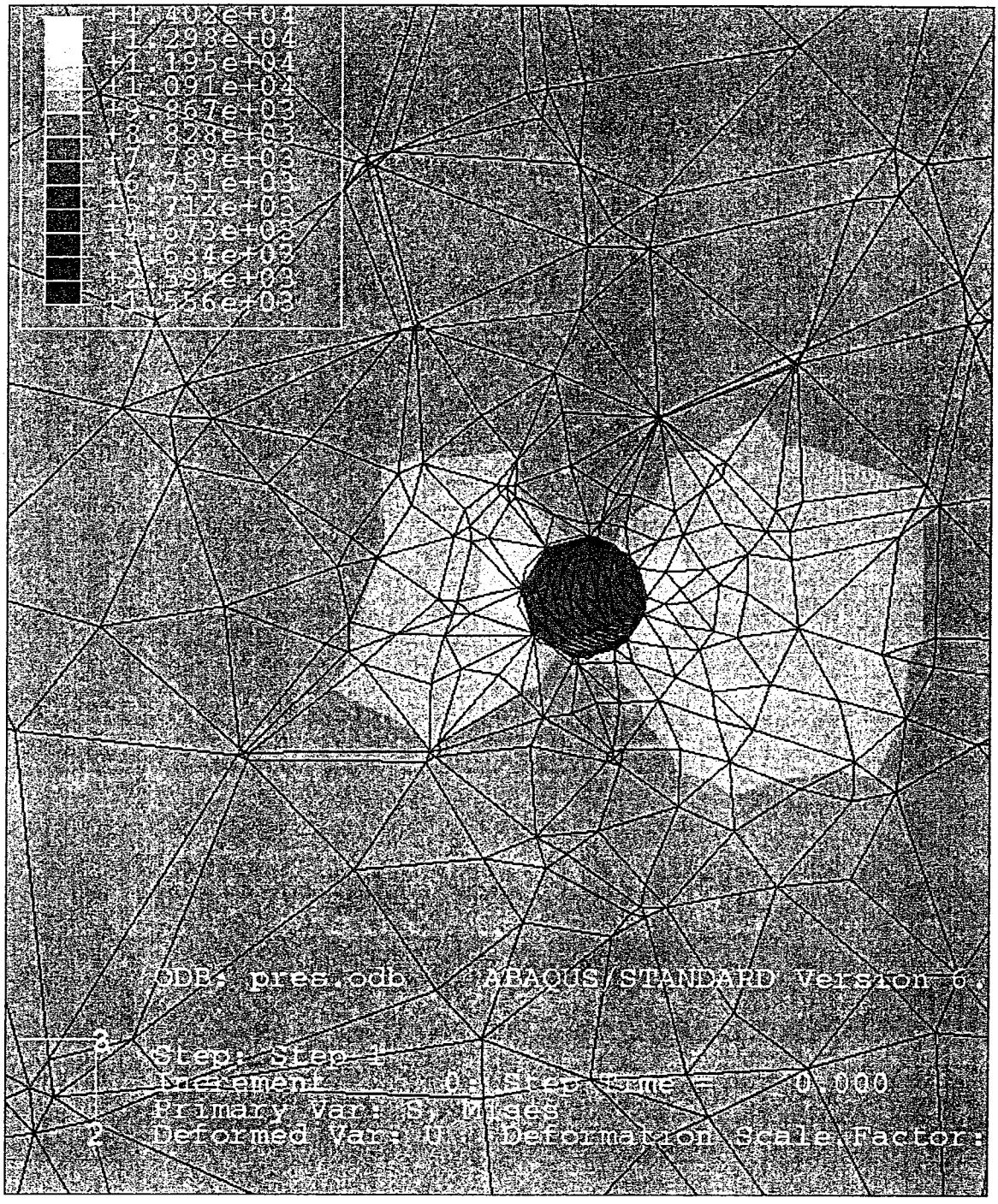

Figure 4. 2 Stress distribution of inclined pile under pullout load-Present Study[3]

[3] A comparison can be drawn for cross-sections between Figure 4.1 and Figure 4.2 with respect to stress distribution

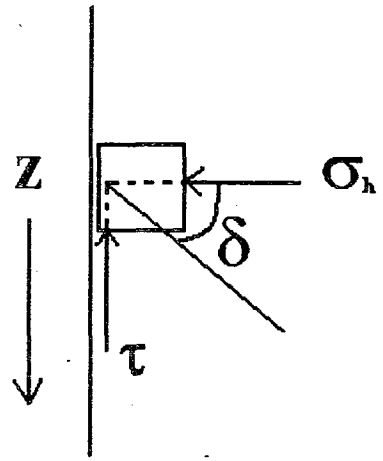

Figure 4. 3 Pile-Soil friction force equilibrium

Shaft resistance Qs equals vectorial resultant of horizontal and frictional pressure.

$$Q_s = c\int_0^L \tau.dz \tag{4.1}$$

$$\tau = \sigma \tan\delta \tag{4.2}$$

c as perimeter, Equation 4.1 becomes;

$$Q_s = c\int_0^L \sigma_h \tan\delta.dz \tag{4.3}$$

It is required to assume δ is constant although it changes with depth. But this variation could be reduced to an average value. However in calculation of shaft resistance we have considered this variation in dimension factor values which associates with soil friction angle δ and L/D.

$$\sigma_h = K\sigma_v \tag{4.4}$$

Horizontal value of earth pressure can be defined as equation 4.4 presents.

Equation 4.1 becomes as Broms (1966) proposed a general formula to predict the vertical shaft capacity of a single pile.

$$Q_s = c\int_0^L (K_z \tan\delta_z \sigma'_{vz})dz \qquad (4.5)$$

where σ'_{vz} is effective vertical stress at depth z; δ_z mobilized angle of friction on the pile-soil interface at a depth of z; K_z is coefficient of earth pressure at depth z; c pile perimeter and L, length of pile.

Later studies simplify the equation as follows;

$$Q_s = cK_s \tan\delta_m \int_0^L \gamma' z dz \qquad (4.6)$$

where Ks is average coefficient of earth pressure acting on pile shaft, δ_m average mobilized angle of friction on the pile-soil interface, and γ' effective unit weight of sand.

During application of load, pile-soil membrane shifts with movement resulting changes in soil character and measured parameters. Abaqus can provide correlation between parameters. Hence we defined "Dimension Factor, B" to overcome this issue.

Table 4.1 illustrates Dimension Factor values versus Reduction Factor. We reduce the shaft resistance according to friction angle and diameter due to pressure on soil-pile membrane.

Table 4. 1 Dimension Factor Values, B vs Friction Angle, ϕ-Present Study

B	0	0.1	0.2	0.3	0.4	0.5	0.6	0.7	0.8
ϕ	Reduction Factor								
20	0.65	0.72	0.75	0.8	0.82	0.84	0.87	0.9	0.93
30	0.45	0.55	0.58	0.63	0.68	0.72	0.76	0.8	0.83
40	0.29	0.33	0.35	0.43	0.5	0.55	0.63	0.7	0.78

As seen here, Figure 4.4 demonstrates relationship between pile length and diameter. Here dimension factor correlates length and diameter ratio to soil character as Table 4.1 illustrated.

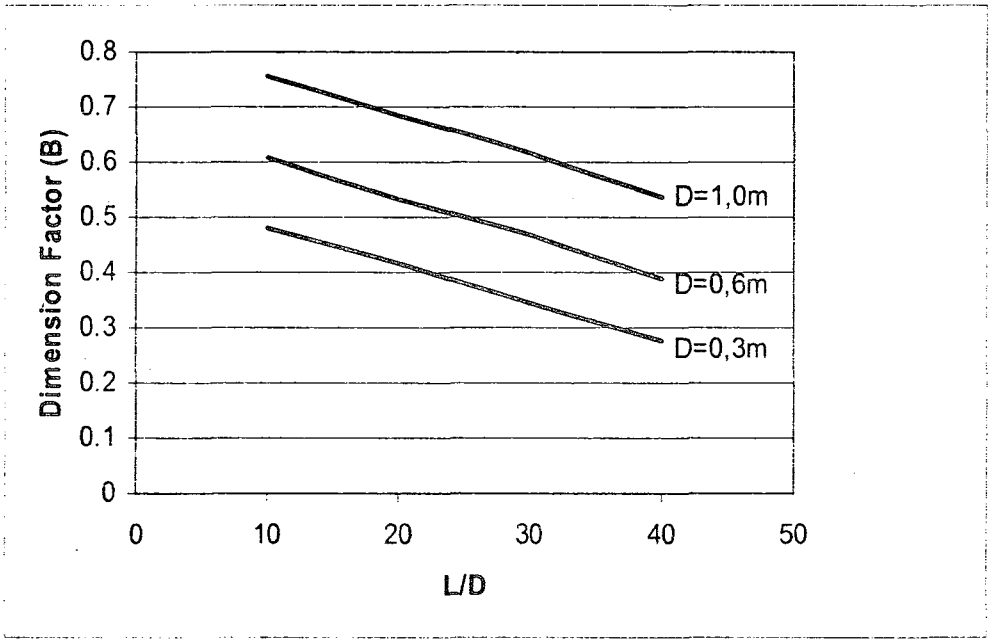

Figure 4. 4 Dimension Factor vs L/D-Present Study

4.2 SHAFT RESISTANCE CALCULATION PROCEDURE

Shaft Resistance formula

$$Q_s = cK_s \tan(B\phi) \int_0^L \gamma' z dz \qquad (4.8)$$

Hence, the procedure of calculating shaft resistance can be summarized as follow;

1. Given the diameter and length of the pile refer to Figure 4.4 to find dimension factor, B.
2. Assume movement is completed
3. Knowing values of ϕ and inclination angle α obtain coefficient of earth pressure K from Figure 4.5 Consider the pile shape as well.
4. Determine Reduction Factor, R from Table 4.1
5. Find K_s=RK

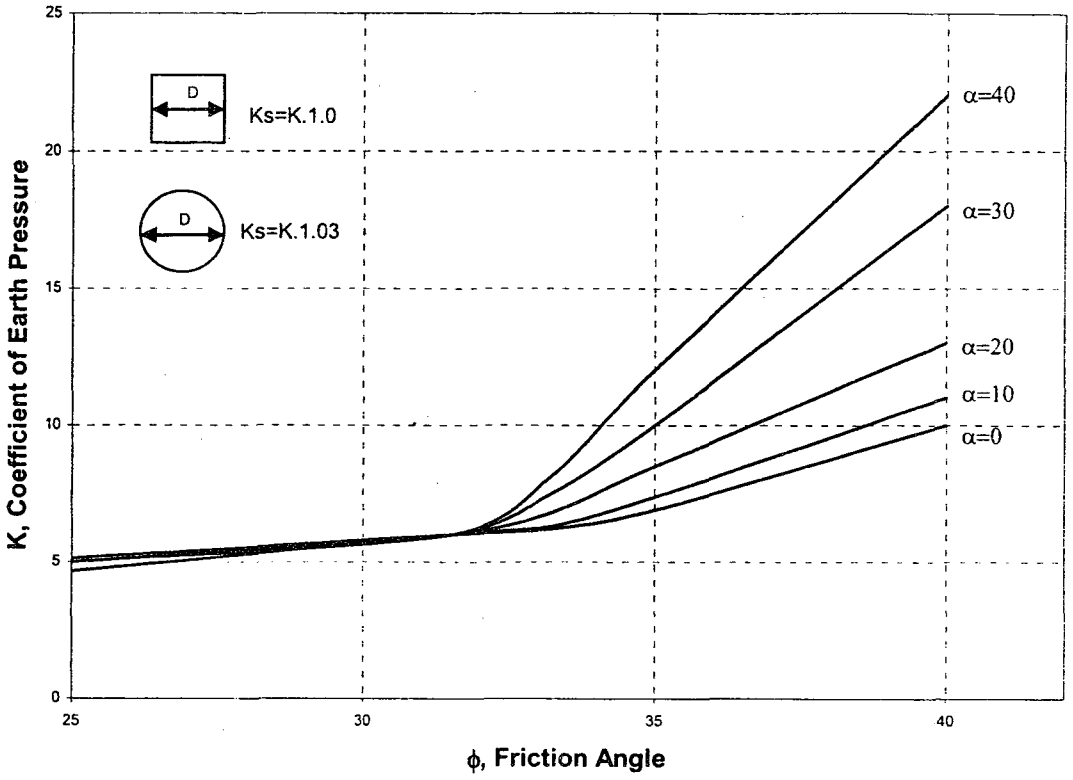

Figure 4. 5 Friction Angle vs K values for round and square pile-Present Study

4.3 VERIFICATION OF DESIGN CHARTS

The method verified according to the previous test results presented. The method can be used in real-size piles. Results are as follows.

Example

Table 4. 2 Field values for of Jonesville Lock and Dam Sherman

Test					Unit Weight	Pile Capacity	Present Method
No	D (m)	L/D	ϕ	α (inclination)	kN/m3	kN	kN
C-1	0,46	25,25	37	0	12,3	1128	1088

D: D=0.46m

c=0.46π=1.44m

L=11.73m

L/D=25.25

B=0.40 (Figure 4.1)

K=7*R2=7*1=7 (Figure 4.2)

for B=0.40

R=0.52 (Table 4.1)

Ks=K*0.52=6.5*0.52=3.38

$$Q_s = cK_s \tan(Bx\phi) \int_0^L \gamma' z dz$$

$$Q_s = 1.44x3.38\tan(0.4x37)\left[\frac{11.73^2}{2} - 0\right]12.3 = 1088\text{KN}$$

Result obtained from analytical method stays in 7% error band which is reasonably accepted for actual results.

4.4 LIMITATIONS FOR DESIGN PROCEDURE

1. Due to generalized model components of the analysis and design charts, some limitations on design procedure will apply. According to our assumptions in model development, gradual loading is one of the limitations. Basis of loading must comply with small-sliding principle. Therefore, an additional factor for sudden impact loading must be considered in design.

2. Another limitation is uniformity of soil. In an ideal environment, soil particles on pile membrane must contact to build friction module for resistance. Transitions on soil characteristics will affect dimension factor with respect to unit weight of soil.

3. Calculation procedure is valid for driven concrete piles.

CHAPTER V

5.1 CONCLUSION

A 3D model is developed to examine the case of a single pile embedded in sand. The results obtained by the model were validated by the available experimental and field results in the literature. A design method is suggested to determine shaft resistance for uplift and compression loadings. The followings are concluded;

1. With an increase at inclination α angle slightly reduces shaft capacity due to decrease in mobilized angle of friction.
2. Friction angle $\phi = 32^{\circ}$ and smaller shaft resistance does not greatly influenced by inclination of pile.
3. Shaft resistance is highly dependent on pile length, diameter, friction interface angle, pile shape, and initial loading conditions.
4. Pile capacity at uplift is less than for compression loading (when tip resistance and weight of the pile are neglected).
5. In 3D models, gravity is a major parameter one has to consider. In addition, degrees of freedom of nodes affect shaft resistance dramatically. Therefore one side of acting force on soil part acts freely while the other restraint by encastre elements.
6. Design charts are presented to estimate load capacity of single pile in sand.
7. Calculation method shows great resembles to values obtained from field work.

5.2 RECOMMENDATIONS FOR FUTURE RESEARCH

1. For a 3D model predefined hole seems like the only solution gives results, due to huge displacements in nodes triggering insolvable systems, other means should be considered.
2. A critical depth study can be conducted for 3D battered piles.
3. Presence of water can be taken into account.
4. Cap plasticity models will give better results once all the parameters were obtained from literature.
5. Tetrahedron meshing is thus far the best approach for irregular systems. Using brick elements will increase computation time and affect the results of analysis.
6. Bored piles are rather difficult to model where gravity loading is a concern on soil particle to reproduce initial soil condition.

BIBLIOGRAPHY

1. ABAQUS Inc. *ABAQUS Documentation*. Vol. 6.6.1. Internet: 2006, http://abaqus.custhelp.com/cgi-bin/abaqus.cfg/php/enduser/home.php.

2. Alawneh, Ahmed Shlash. "**Tension Piles in Sand: A Method Including Degradation of Shaft Friction during Pile Driving.**" *Transportation Research Record* no. 1663 (1999): 41-49.

3. Alawneh, Ahmed Shlash, Abdullah I. Husein Malkawi, and Husein Al-Deeky. "**Tension Tests on Smooth and Rough Model Piles in Dry Sand.**" *Canadian Geotechnical Journal* 36, no. 4 (1999): 746-753.

4. Alawneh, Ahmed Shlash, Osama K. Nusier, and Mustafa Al-Kateeb. "**Dependency of Unit Shaft Resistance on in-Situ Stress: Observations Derived from Collected Field Data.**" *Geotechnical and Geological Engineering* 21, no. 1 (2003): 29-46.

5. Ergun, M. U. and H. Akbulut. "**Bearing Capacity of Shaft-Expanded Driven Model Piles in Sand.**" *Geotechnique* 45, no. 4 (1995): 715-718.

6. Foundation Failure. 22 Jan. 1999. Wireless Estimator. 17 July. 2008. <http://www.wirelessestimator.com/wifi/images/uploads/FoundationFailure.gif>

7. Gavin, Kenneth G. and Barry M. Lehane. "**The Shaft Capacity of Pipe Piles in Sand.**" *Canadian Geotechnical Journal* 40, no. 1 (2003): 36-45.

8. Hanna, A. M. and A. Afram. "**PULL-OUT CAPACITY OF SINGLE BATTER PILES IN SAND.**" *Canadian Geotechnical Journal* 23, (1986): 387-392.

9. Hanna, A. M. and Nguyen T. Q.. **"Shaft Resistance of Single Vertical and Batter Piles Driven in Sand."** ASCE, *Journal of Geotechnical and Geoenvironmental Engineering* 129, no. 7 (2003): 601-607.

10. Helwany, Sam. ***Applied Soil Mechanics with ABAQUS Applications***. 1st ed. USA: John Wiley & Sons, 2007.

11. Jardine, R. J. and R. F. Overy. **"Axial Capacity of Offshore Piles Driven in Dense Sand."**Offshore Technol Conf, Richardson, TX, USA, May 6-9 1996, 1996.

12. Kraft, Leland M.,Jr, Joseph N. Suhayda, Steven C. Helfrich, and Justo E. Marin. **"Ocean Wave Attenuation due to Soft Seafloor Sediments."** *Marine Geotechnology* 9, no. 3 (1990): 227-242.

13. Leathers, Francis D. **"Deformations in Sand Layer during Pile Driving."**Publ by ASCE, New York, NY, USA, Jun 16-18 1994, 1994.

14. Mansur, C. I., and Kaufman. R. I. (1956). " **Pile Tests, Low-Still Structure, Old River, Lousiana.**" Trans., ASCE, 123, pp(715-743).

15. Massoud, Nabil Fahim. **"Shear Strength Chracteristics of Sand** ." M. Eng, Concordia University, 1981.

16. Meyerhof, G. G. **"Ultimate Bearing Capacity of Footings on Sand Layer Overlying Clay**." *Canadian Geotechnical Journal* 11, no. 2 (1974): 223-229.

17. Pise, P. J. and B. C. Chattopadhyay. **"Uplift Capacity of Driven Piles in Sand."** *Journal of the Institution of Engineers (India), Part CI: Civil Engineering Division* 68, no. 2 (1987): 89-91.